THE JOURNAL OF PHYSICAL CHEMISTRY C
A JOURNAL OF THE AMERICAN CHEMICAL SOCIETY

pubs.acs.org/JPCC Review Article

Recent Developments on Molten Salt Synthesis of Inorganic Nanomaterials: A Review

Santosh K. Gupta and Yuanbing Mao*

Cite This: https://dx.doi.org/10.1021/acs.jpcc.0c10981 Read Online

ACCESS | Metrics & More | Article Recommendations | Supporting Information

ABSTRACT: A wide range of inorganic nanomaterials with many fascinating properties and application potentials in widespread fields may be synthesized by wet chemical synthetic routes. To achieve scientific and commercial viability of nanomaterials with uniformity and scalability, it is necessary to develop efficient and cost-effective, preferably sustainable, methods. The molten salt synthesis (MSS) method is one such bottom-up technique to fabricate a wide variety of inorganic nanomaterials with tunable size, morphology, and surface characteristics. It is also environmentally friendly, cost-effective, simple to operate, easy to scale, and generalizable, etc. This review gives a critical overview on this emerging and rapidly developing method for making defect free nanomaterials in well-defined texture, surface, and morphology at a relatively low formation temperature. We have discussed its different aspects, including the role of molten salts, the choice of molten salts, the electrochemical aspects, some advanced modifications of the conventional MSS technique, and their implications. To show the most recent development on MSS synthesized inorganic nanomaterials, this review only encompasses the studies reported over the last six years (2015−2020). We have summarized technologically important and emerging families of inorganic nanomaterials such as metal oxides, fluorides, nitrides, silicides, chalcogenides, oxohalides, borides, and carbides. Finally, a few perspectives for the MSS method are highlighted. It is expected that this review will further attract scientists to explore the MSS method in making size- and shape-tunable nanomaterials.

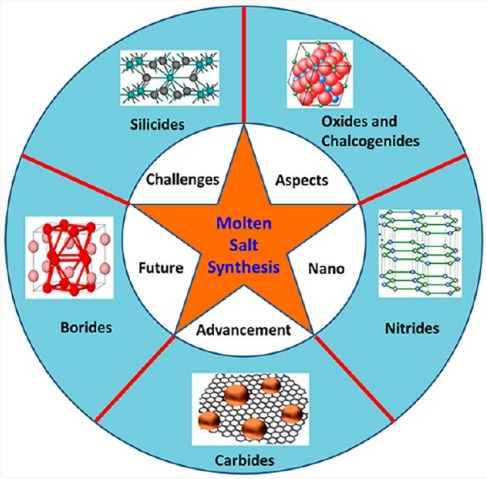

1. INTRODUCTION

Materials science has been playing a more and more pivotal role in our life with material functionalities tailored by precise synthesis control.[1−3] Synthesis methods and parameters inevitably dictate the structure, crystallinity, particle size, morphology, porosity, texture, and surface among other characteristics of materials, which are extremely critical in tailoring their properties.[4] From an engineering perspective, material synthesis methods should also be reliable, sustainable, and economic.[5] Chemistry plays the fundamental role in controlled synthesis of functional materials.[6] There are many recent exemplary material inventions,[7−19] and all of their properties and applications strongly depend on synthesis methods.[20−26]

Nanomaterials, having at least one dimension falling in the size range of 1−100 nm, are among the top priority of advanced materials.[27−31] They possess significantly different properties from their bulk counterparts due to a high surface to volume ratio (S/V) and possibly quantum effect.[32] Their physicochemical properties are manifested mainly by atomic physics rather than the classical physics which govern bulk materials.[33−36] Their size-tunable properties have inspired intense scientific curiosity and technological applications in the recent couple of decades.[27,29,33,35,37,38]

By the same token, synthesis methods play a huge role in designing nanomaterials.[24−26,39,40] Their controlled synthesis mainly focuses on optimizing size, shape, composition, surface, defect, architecture, dimension, etc.[41,42] Several common synthesis techniques of nanomaterials include sol−gel, combustion, solvothermal, hydrothermal, sonochemical, microemulsion, polyol, coprecipitation, and molten salt synthesis (MSS), etc.[1,28,43−52] Table S1 summarizes the advantages and disadvantages of a few widely used synthesis methods for inorganic nanomaterials along with the solid-state route (SSR) for comparison.

Among the synthesis methods for nanomaterials, the MSS stands out as a unique technique.[44] It can be considered as a modified version of the SSR in a way that a salt is added as a solvent once melted to assist in dissolving solid reactants and solvating ions by strong polarization and rapid movement of

Received: December 8, 2020
Revised: January 29, 2021

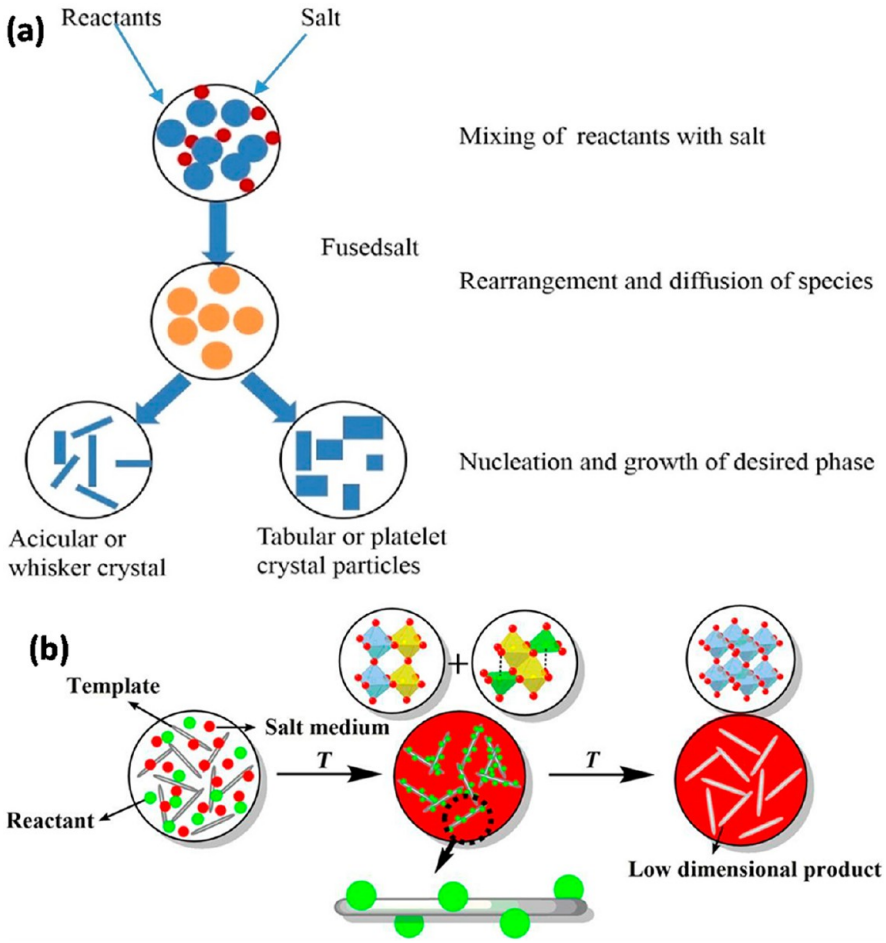

Figure 1. Schematic showing synthesis steps for inorganic crystals involved in (a) the MSS (Copyright 2017. Reproduced with permission from Elsevier)[83] and (b) the TMSS (Copyright 2020. Reproduced with permission from the Royal Society of Chemistry).[85]

reactant species through convection and diffusion.[53] The molten salts help achieve phase pure products with homogeneous powder characteristics and controlled size/shape at relatively low temperature compared to the SSR.[54] It offers advantages including being simple to operate, exhibiting rapid product formation, facilitating large scale production, being cost-effective, having low product defect density, a ligand free surface, and reproducibility, and being environment friendly.[32,35,38,55−61] Nanomaterials synthesized by the MSS method are generally highly homogeneous and phase pure, having controlled size and morphology, and most of the time, they have the formed particle size being in the range of tens of nanometers.[62]

There have been a few published review articles which cover the MSS and flux syntheses.[52,54,62−67] Most of them focus on special classes of compounds by various synthesis methods and a few by the MSS for various nanomaterials.[44,54,60,62−64,66−70] For example, Patzke et al. compiled several synthesis techniques designated for oxide nanoparticles along with mechanistic studies.[71] Recently we published an article focusing on the utility of the MSS for a few simple and complex oxide nanomaterials.[52] Some of the review articles specialize on aerosol-assisted MSS (AMSS)[68,72−75] and topochemical MSS (TMSS)[62,76−79] techniques as further discussed below. Considering as a fast-growing research area, the MSS is lack of an updated general review for a broad range of nanomaterials. To avoid redundancy and present the most recent development in the MSS field for the synthesis of inorganic nanomaterials, we have only included studies published in the past 6 years (2015−2020) in the present contribution after a systematic survey of the literature.

More specifically, we started this article with a general discussion of the MSS method, especially its importance and the role of molten salts for synthesizing nanomaterials. We then discussed various MSS processing parameters to be considered for preparing high quality nanomaterials. We also assessed the advantages and disadvantages of the MSS. More importantly, we surveyed the literature and categorized the MSS synthesized nanomaterials based on their chemical composition into metal oxides, borides, carbides, nitrides, fluorides, silicides, chalcogenides, and oxyhalides. We also introduced some advanced MSS techniques, such as the TMSS, AMSS, and kinetically modified MSS during our discussion. Finally, we concluded this review on the MSS for inorganic nanomaterials along with its perspective. We tried to give a full spectrum of the MSS method for inorganic nanomaterials (not including elemental ones) in the current article and would like to request forgiveness if we have missed out any relevant reports.

2. UNIQUE FEATURES OF THE MSS

2.1. Basic Synthesis Principles. Fundamentally the MSS method is a solvent-based synthetic route where chemical

https://dx.doi.org/10.1021/acs.jpcc.0c10981
J. Phys. Chem. C XXXX, XXX, XXX−XXX

reactions take place in fluxes of salts with relatively low melting points. Such molten salts act as solvents and facilitate efficient diffusion and reaction of reacting species.[80,81] In principle, the MSS method is different from the flux method as the former uses molten salts as solvents where the latter employs salts as additives of reaction mixtures.[82] Accordingly, a smaller fraction of salts is used in the flux method compared to the MSS method.

In general, the MSS method involves stages of mixing, diffusion, nucleation, and growth (Figure 1a).[83] Specifically, the first stage involves mixing of precursors with the salt(s) of choice. The second stage goes by heating the above-mentioned mixture at temperatures above the melting point of the chosen salt(s) to form a molten flux. The final stage proceeds by the nucleation and growth of product particles. The increased chemical reactivity of precursors in molten salts is attributed to the enhanced ionic mobility (diffusion rate on the order of 10^{-5} to 10^{-8} cm^2 s^{-1}) and contact area of reactants in the presence of molten salts.[84] On the other hand, the TMSS method (Figure 1b) employs asymmetric reactants with weak solubility in chosen molten salts as template, and therefore, one can control the morphology of designated products via the recombination of local basic unit.[85] Compared with the conventional MSS, the TMSS has the additional advantage for more easily controlling the size and shape of produced particles.[62,86,87] For example, the TMSS was found to be extremely efficient to synthesize low-dimension symmetrically oriented ferroelectrics which is otherwise difficult to obtain from general chemical synthesis methods.[70,88]

2.2. Advantages. The advantages associated with the MSS, especially compared with the traditional SSR, include: (1) enhanced rate of reaction and low product formation temperature endowed by large contacts area between reacting molecules and their increased mobility in the liquid molten salt, (2) highly homogeneous product formed, (3) powder particles with controlled size and shape, and (4) low particle agglomeration degree of the final product.[44,54,63,65−67] Its other advantages include scalability, simplicity, generalizability, ease to conduct, etc.

The products formed by the MSS are highly crystalline in nature and have well-defined facets even though reactions take place at lower temperatures and shorter time compared to the SSR.[89] Moreover, crystals grown by the MSS at lower temperature lead to phase pure products without unwanted and unstable high temperature phases or irreversible phase transformations that are otherwise very difficult to achieve.[64,82] MSS can also lead to stabilization of incongruently melting and highly nonstoichiometric mixtures.[64,82,89,90] The flux-aided crystal growth takes place in the absence of thermal gradient, and hence, the formed crystals are in general of high quality and free from defects, vacancies or dislocations.

2.3. Limitations. One of the possible issues of the MSS is sometimes the used molten salts either react with reaction vessels or get incorporated into the final products. For example, salts such as alkali/alkaline earth metal hydroxides and PbO are often used in the MSS owing to their high oxo-basicity, but they tend to cause corrosion to Al and Pt reaction vessels.[54] The caused erosion of the Al and Pt reaction vessels surface may further contaminate the final products. Flux/salt ions would be incubated into products either as flux inclusion inside crystals or as part of crystals themselves. The former can reduce product crystal quality whereas, in the latter case, crystals can acquire unwanted chemicals and structures. To avoid these issues, the analogy of common ion effect has been considered by using salts with common ion existing in the final intended products.[64,82,89−91] For example, to synthesize Cu^+-containing mixed-metal oxides such as $CuNb_3O_8$, $Cu_2Nb_8O_{21}$, $Cu_5Ta_{11}O_{30}$, and $Cu_3Ta_7O_{19}$ by the MSS, using salts of alkali metal halides/carbonates/hydroxides leads to the formation of unwanted phases of $NaBO_3$ and $Na_2B_4O_{11}$ (B = Nb, Ta). Hence, it was found that CuCl is the best salt for the synthesis of these products using the MSS method.[92−101] Most of the salts used in the MSS are abundant and inexpensive. However, in the large-scale production of nanomaterials by the MSS, cost can go up with the large amount of used salts, especially the ones containing expensive lithium metal.

2.4. Safety Considerations. There would be some safety concerns as some salts used, e.g., metal fluorides, can cause skin/eye irritations and cause damage to human tissues as well. Hence, proper care should be taken while employing fluoride-based molten salts. Some salts are either acidic or alkaline in nature, such as $AlCl_3$ and KOH, respectively, which can cause corrosion. Heavy metals consisting of salts such as $BaCl_2$ or BaF_2 are known to harm humans. They are to be processed carefully with all protections. It is better to avoid using salts having high vapor pressures such as $BaCl_2$, CsI, and $ZnCl_2$ unless closed systems are used for carrying out the reactions. Moreover, when the precursor and salt mixture is heated around the T_m of the salt, toxic fumes of NO_x and SO_x would be produced. They are extremely harmful if inhaled. Hence it is better to carry out the MSS in well ventilated fume hoods. To ensure safety from corrosive and toxic fumes, personnel performing the reactions should also wear masks, gloves, goggles, and other protective gears.

3. CRITICAL PROCESSING PARAMETERS OF THE MSS

The critical processing parameters of the MSS method for nanomaterials, which are discussed further below, include (i) the identity of selected salts, (ii) the salt to precursor ratio (SPR), (iii) the MSS operating temperature (MOT), and (iv) the solubility of precursors in the selected salts when melted.[44,82,102,103] Similar to other synthesis methods, parameters such as the characteristics of precursors, heating rate, and processing time also play important roles for the MSS of nanomaterials, while no further elaboration is provided in this review.

3.1. Salt Identity. There are a few essential criteria to be considered as favorable salts used for successful MSS of nanomaterials. They should (a) have a low melting point, (b) be compatible with reactants, (c) possess high aqueous solubility for easy removal after synthesis by simply washing with water, (d) have high thermal and chemical stability, (e) be nontoxic, inert, cheap, and easily available, and (f) have low vapor pressure to avoid evaporation loss during operation.[54,64−66] Depending upon synthesis conditions and compatibility, individual salts or their mixtures can be used. Li et al. have compiled a table with the choices of templates and salts used in the MSS of perovskites with different morphologies such as rods, plates, and spheres, etc.[62] Boltersdorf et al. have also tabulated several commonly used salts along with their melting temperature (T_m) and the synthesized metal oxides.[54]

https://dx.doi.org/10.1021/acs.jpcc.0c10981
J. Phys. Chem. C XXXX, XXX, XXX−XXX

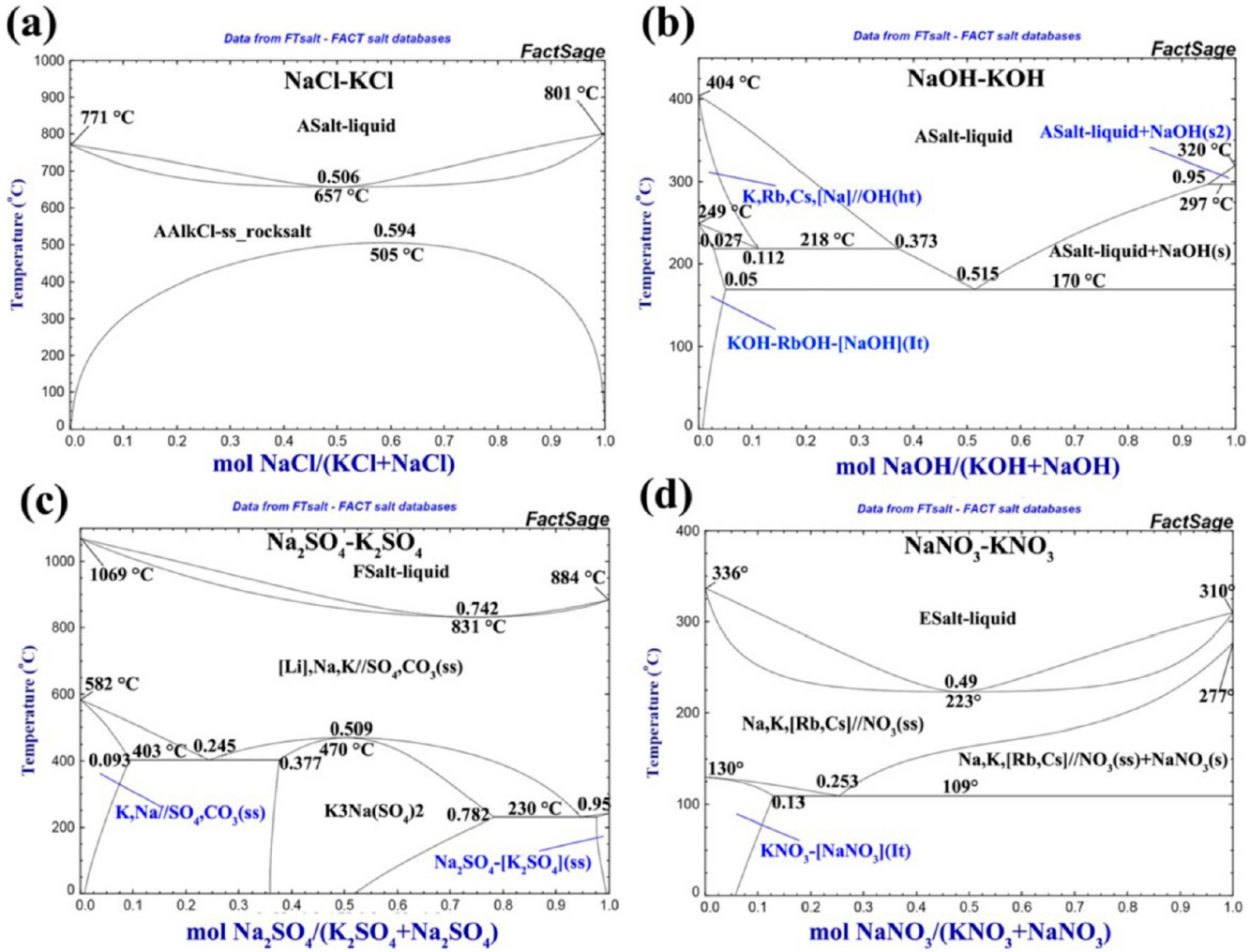

Figure 2. Thermodynamic phase diagrams of the commonly used molten salt systems of (a) NaCl-KCl, (b) NaOH-KOH, (c) Na_2SO_4–K_2SO_4, and (d) $NaNO_3$–KNO_3.[85] Copyright 2020. Reproduced with permission from the Royal Society of Chemistry.

It needed to be emphasized that the MSS reaction temperature is higher than the T_m of the used salt in the synthesis. The decrease of T_m can be achieved by mixing two or more salts in a proper composition to obtain a eutectic composition, which also provides a wider operating temperature range. The most commonly used salts in the MSS include metal halides and oxosalts (such as hydroxides, nitrates, and sulfates) (Table S2).[66] In most of the MSS, it is the eutectic mixture of salts which is preferred due to the reduced T_m and lower viscosity instead of individual salts.[54] For instance, the melting temperatures of NaCl and KCl are 801 and 770 °C, respectively. The eutectic composition of 0.5 NaCl–0.5 KCl has a T_m of 650 °C. Some other eutectic composition examples have been widely employed during the MSS, e.g., 0.635 Li_2SO_4–0.365 Na_2SO_4 with a T_m of 594 °C. Thermodynamic databases are quite helpful in selecting suitable molar ratio and T_m of eutectic mixtures of salts, for example, which can be deciphered from the École Polytechnique de Montréal FactSage FT salt thermochemical software and database.[104] Fu et al. discussed in details the thermodynamic phase diagrams of some of the commonly used molten salts such as NaCl–KCl, NaOH–KOH, Na_2SO_4–K_2SO_4, and $NaNO_3$–KNO_3 (Figure 2a–d).[85] The choice of molten salts for the MSS of particular materials is dictated by the hard–soft acid base (HSAB) concept, Lux–Flood theory, and other reaction conditions.[64,66,105,106] In general, one may want to avoid using molten salts having borate, phosphate, or silicate moieties, as the covalent nature of such anionic groups leads to highly viscous liquids and vitreous phases. Several other types of molten salts have been used to synthesize some specific material systems such as peroxides, chalcogenides, chalcophosphate, hydrofluxes, and metals/intermetallics.[66,105,107−115] For instance, Bugaris et al. exploited the preparation of peroxides, superoxides, borates, tungstates, molybdates, and vanadates of alkali and alkaline earth metals with bismuth oxide, lead oxide, and lead fluoride as molten salts.

One of the most frequently employed molten salt systems, metal oxosalts, is considered to give decent bases, and therefore, the metal oxosalts can serve as oxidizing agents and oxygen donors. When oxosalts are used in the MSS, the Lux-flood type equilibrium is as follows:[105,116]

$$\text{oxobase} \leftrightarrow \text{oxoacid} + O^{2-} \quad (1)$$

where O^{2-} acts as a base. The basicity of a molten salt is defined as $pO^{2-} = -\log m(O^{2-})$. Its value determines the kinetics of the MSS. For example, at moderate basicity (pO^{2-}), TiO_2 crystal precipitates via electrochemical reaction

https://dx.doi.org/10.1021/acs.jpcc.0c10981
J. Phys. Chem. C XXXX, XXX, XXX−XXX

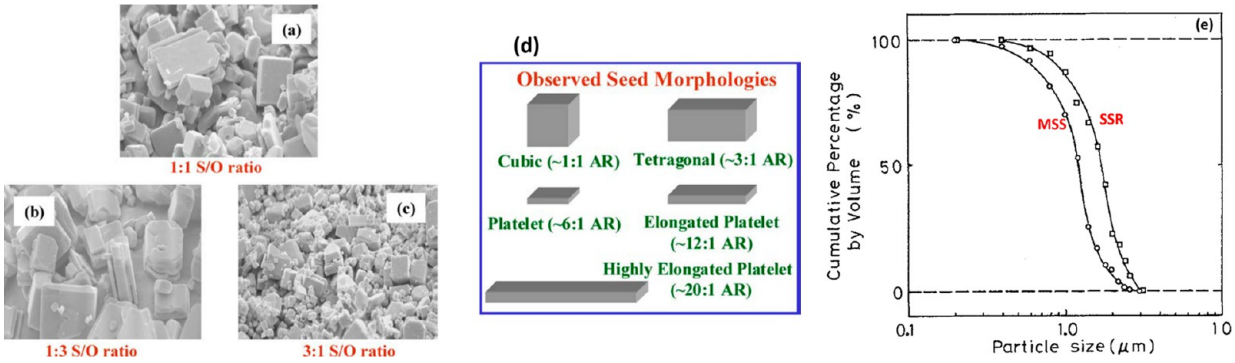

Figure 3. Effects of (a–c) SPR on morphology and (d) heating temperature on shape and aspect ratio of $Sr_3Ti_2O_7$ particles where S/O represents the salt to oxide ratio.[128] Copyright 2006. Reproduced with permission from Springer Nature. (e) Particle size distribution of $BaTiO_3$ powders obtained by the MSS and the SSR.[129] Copyright 1986. Reproduced with permission from Springer Nature.

(eq 2) whereas titanate ion precipitates out at lower pO^2 via eq 3:

$$Ti^{4+} + 2O^{2-} \rightarrow TiO_2 \quad (2)$$

$$TiO_2 + O^{2-} \rightarrow TiO_3^{2-} \quad (3)$$

So, by tuning the basicity of molten salts, one can either have titania or titanate ion as final products. Other salts can also be the preferred options of molten salts, such as metal chalcogenides and chlorates. For example, Banerjee et al. have reported the synthesis of unusual polysulfide phases such as $KSnPS_4$, $RbSnPS_4$, and $CsSnPS_4$ using chalcophosphate as the molten salt.[117] Here metal chalcogenides not only act as chalcogen donors but also control the texture and structure of the products.[118,119] In cases where high oxidation states need to be stabilized, metal chlorates are good molten salt choices while one should be mindful about their explosive nature.[120]

Combinations of salts with different anionic components have also been used to synthesize various compounds as heterogeneous salt mixtures can shift the acid–base equilibrium for the preferential precipitation of targeted compounds. For example, $LiMn_2O_4$ can be synthesized using a chloride–carbonate salt mixture.[121]

In some of the synthesis, the used molten salts not only act as flux but also play the role of ion-donors. For example, in the synthesis of $ZnEu_2Ti_3O_{10}$, Zn^{2+} is provided by $ZnCl_2$ which was used as the flux.[122] The product $ZnEu_2Ti_3O_{10}$ was formed by the ion-exchange process between $K_2Eu_2Ti_3O_{10}$ and $ZnCl_2$ via TMSS.

3.2. SPR. SPR plays an important role in the MSS method. Its value is basically decided by the facts that how much interstitial space is there in the precursor(s) and how much is needed to cover the surface of reacting precursor species. When the SPR is too small, the implication of the liquid phase of used molten salts is not fully expected. On the other hand, if it is too high, there can be two main issues. First, the precursor particles get separated as sediments.[121] This separation is attributed to different sedimentation rate of the precursor molecules due to their distinct size and density, which ultimately affect the rate of reaction. Second, excess salts from the precursor and salt mixture would fail to hold the entire salt molecule together, owing to limited availability of interstices. These salts which came out of the precursor and salt mixture no longer act as a solvent. Moreover, such salts stick to the wall of the alumina/SiC crucible and get converted to a hard solid mass, and dissolution of such a filthy mass is very tedious.[82]

Moreover, the addition of molten salts enhances the reaction rate during the MSS as compared to the SSR. Recent kinetic investigation by X-ray diffractions (XRD) measurements has thrown remarkably interesting results on the enhanced rates of chemical reaction and crystal formation in the case of the MSS compared to the SSR. The reaction time for the formation of several metal oxides such as $NaTi_2O_4$, $CuNb_3O_8$, and $RbCa_2Nb_3O_{10}$ was found to be reduced from 24 to 96 h in the SSR to as low as 15 min in the MSS.[92,96,97,100,123−125]

SPR also affects the size of synthesized particles.[126] However, the size of the synthesized particles by the MSS would not be monodispersed even when all reacting species have been dissolved in the used molten salts. For example, it was found that two different sizes of plate-like bismuth tungstate particles (i.e., of the order of several micrometers and approximately around 100 μm) were formed depending upon the value of SPR and heating conditions using bismuth and tungsten oxides as the precursors in a NaCl–KCl eutectic mixture.[127] The same thing happened to the morphology of $Sr_3Ti_2O_7$ particles due to the effect of SPR (Figure 3a–c).

3.3. MOT. The main purpose of heating precursor and salt mixtures is to shorten the diffusion length and increase the transport rate of reacting species to reacts during the MSS. The diffusion length is reduced greatly in the MSS compared to the SSR. MOT of the MSS basically depends on two main factors: (i) temperature at which salts decompose and (ii) the vapor pressure of salts. It has profound influence on size, shape, and aspect ratio of powder particles as exemplified by the formed $Sr_3Ti_2O_7$ particles with the observed seed particles formed at different temperatures (Figure 3a–d).[127,128,130]

The main reason behind the higher degree of agglomeration by the SSR is due to the concurrent occurrence of product sintering and formation.[131] On the other hand, the particle surface is well covered by molten salt in the MSS, which avoids neck formation between product particles and hence leads to a lower degree of agglomeration. The size distribution of the formed $BaTiO_3$ particles by these two methods from the same $BaCO_3$ and rod shape TiO_2 as the precursors (Figure 3e) clearly displayed that the particles synthesized by the MSS had a narrower size distribution compared to those synthesized by the SSR.[129] This difference

https://dx.doi.org/10.1021/acs.jpcc.0c10981
J. Phys. Chem. C XXXX, XXX, XXX−XXX

was attributed to a larger degree of agglomeration in the particles synthesized by the SSR.

3.4. Solubility. The rate of the MSS reactions is highly proportion to the solubility of precursors in the selected molten salts as they determine the amount of precursors that can be accommodated by the molten salts. For metals, neutral precursors and gaseous molecules, molten salts served as excellent solvents at high temperatures.[66] Solubility of metal oxides in molten salts depends on the closeness in various physicochemical properties between solute and solvent such as electronegativity, polarizability, nature of bonding, common ion effect, etc.[54] Solubility of various metal oxides in molten salts has been investigated previously using several thermodynamic and potentiometric methods.[132−141]

Most of metals are soluble in their halide salts and are completely miscible above a specific temperature. The solubility depends on many factors such as atomic size, electronegativity, polarity, etc. Solubility of metal oxides in molten salts varies significantly from less than 1×10^{-10} mole fraction to more than 0.5 mole fraction, typically 1×10^{-3} to 1×10^{-7} mole fraction.[65] Product formation in the presence of solid reactant particles suggests that molten salts are distinct from ordinary solvents, which tend to solubilize most of reactant particles. As a result, this product precipitation in the MSS proceeds via a homogeneous liquid phase.[65] For elements in the same group, their solubility increases with increasing molecular weight. For example, the solubility follows the trend of $SrCl_2$ (25 mol %) > $CaCl_2$ (16 mol %) > $MgCl_2$ (1.1 mol %) at 1000 °C.[142] The number of electrons in the valence shell also dictates the solubility of some metal ions: the one with higher valence state exhibits higher solubility.

Most of the metal oxides are soluble in metal salts at high temperatures, which can be understood from the concept of hard−soft acid−base (HSAB) theory.[54] Molten salts are mostly soft in character, so they prefer interacting with soft/polarizable reactants. The fact that MgO is hard in character causes it to be difficult to dissolve in binary/multinary chloride systems (< 0.05% at 800 °C). On the other hand, softer CaO easily dissolves in $CaCl_2$ (solubility > 15% at 800 °C).

4. METAL OXIDE NANOMATERIALS SYNTHESIZED BY THE MSS

The oxide nanomaterials synthesized by the MSS include low dimensional simple oxides,[54,63,143] perovskites,[62,67] double perovskites,[76,144,145] delaffosites,[146] spinels,[147] and complex quaternary and higher oxides.[64] Here we start with its synthesis of binary oxide nanomaterials.

4.1. Binary Oxides. Our basic knowledge on metal oxides is relatively far from that for metals, and as yet, little is known about the fundamental relationships between their reactivity and chemical composition, crystal structure, and electronic properties.[148−154] Hence, there has been continuous demand on new ways to improve the properties of metal oxides and their nanomaterials. Adjustable MSS parameters for binary oxide nanomaterials such as synthesis temperature, salt/precursor used, and particle characteristics along with their proper citations for several binary oxides have been compiled in Table S3.

It was found that MOT played an important role in tuning the phase as well as the morphology of TiO_2 NPs.[155] The morphology of the synthesized TiO_2 NPs by the MSS changed from nanosheets to nanorods as the MOT was raised from 400 → 450 → 500 °C (Figure 4). At the same time, the crystal phase changed from rutile → anatase → rutile/anatase heterostructure while increasing the MOT from 400 → 450 → 500 °C. The TiO_2 NPs synthesized at 500 °C exhibited the best performance in terms of photocatalytic activity which was attributed to efficient electron−hole separation on rutile/anatase heterostructure.[2]

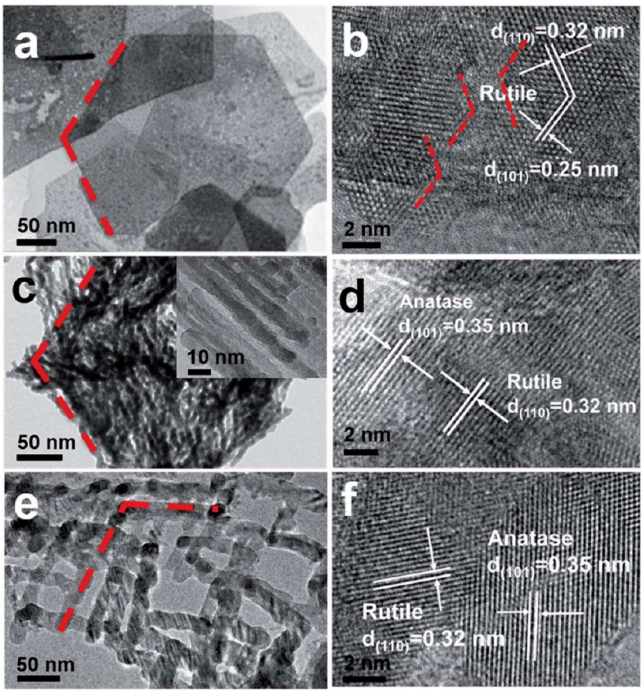

Figure 4. TEM and HRTEM images of TiO_2 NPs prepared with different MOTs: (a, b) 400 °C, (c, d) 450 °C, and (e, f) 500 °C.[155] Copyright 2015. Reproduced with permission from the Royal Society of Chemistry.

Li et al. synthesized NPs of several transition metal oxides such as FeO_x, CeO_2, CuO, ZnO, Co_3O_4, NiO, Ni−Fe−O, Y:CeO_2, and Cu:CeO_2 using a generalized MSS approach (Figure S1).[156] These NPs were formed rapidly at very short time of around 1 min and at an incredibly low temperature of around 100−150 °C. The employed molten salts were $LiNO_3$−KNO_3 and $LiNO_3$−$NaNO_3$−KNO_3−$Ca(NO_3)_2$ whereas Li_2O was used for oxygen source. The formed NPs were monodispersed with low crystallinity and cleaned surface at sub-15-nm size.

Reddy et al. demonstrated CuO quantum dots decorated with TiO_2 nanocomposite using the MSS.[157] Hu et al. explored the MSS for 2D ion-intercalated metal oxides and hydroxides, such as cation-intercalated Mn/W oxides of $Na_{0.55}Mn_2O_{4\cdot1.5}H_2O$, $K_{0.27}MnO_{2\cdot0.54}H_2O$, Li_2WO_4, and $Na_2W_4O_{13}$ and anion-intercalated Cu/Zn oxides of $Zn_5(OH)_8(NO_3)_2\cdot2H_2O$ and $Cu_2(OH)_3NO_3$ with a large lateral size and nanometer thickness in a short time.[158]

Ultrathin sub-5-nm hexagonal WO_3 nanowires were synthesized using a dopant-driven modified MSS with $NaNO_3$ as the molten salt and ammonium molybdate tetrahydrate ($H_{24}Mo_7N_6O_{24}\cdot4H_2O$) as the dopant.[159] The proposed mechanism (Figure 5) suggested that the Mo doping induced collapse followed by the aggregation of nanocluster, coalescence, and reconstruction to form

https://dx.doi.org/10.1021/acs.jpcc.0c10981
J. Phys. Chem. C XXXX, XXX, XXX−XXX

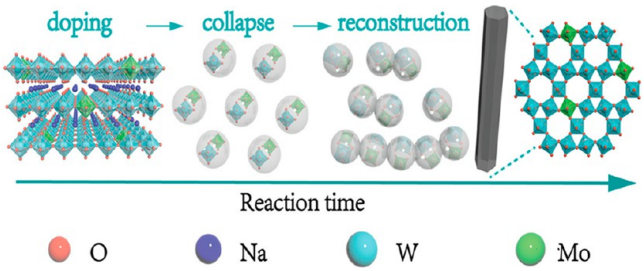

Figure 5. Schematic of the MSS leading to Mo doped ultrathin hexagonal WO_3 nanowires.[159] Copyright 2020. Reproduced with permission from John Wiley and Sons.

hexagonal ultrathin WO_3 nanowires, which could be seen from TEM and HRTEM images (Figure S2).

4.2. Functional Ternary Metal Oxides. One of the most fascinating aspects of the MSS is in the synthesis of complex metal oxides consisting of two cations A and B or more which can be achieve following the general scheme shown in Figure 6. A mixture of solid precursors with A and B ions along with the selected molten salts is thermally treated above the T_m of the salt(s). One can tune the property of final ternary metal oxide nanomaterials by varying the reaction temperature, time, pH, choice of salt, etc.[44,102,160−162] Below we described a few groups of ternary metal oxide nanomaterials by the MSS.

4.2.1. ABO_3-Type Perovskites. Owing to the importance associated with various applications of perovskite materials, high quality synthesis of them in well-defined size and morphology has become widely pursued in recent years.[60,61,67,144,163−173] Our group has worked extensively on synthesis, properties, and application of various perovskite materials in the past two decades.[60,61,144,163,164,168−173] For the MSS of ABO_3-type perovskite nanomaterials, Xue et al. reviewed recent advances on the MSS of low dimensional perovskite nanomaterials.[174] Cheng et al. also published a review on the synthesis of perovskite nanocrystals using the MSS.[175] On a similar line, Wu et al. mentioned several perovskite nanocrystals synthesized by the MSS in their review.[176] Gonell et al. reported the synthesis of various magnetite perovskite nanocrystals using the MSS.[177] There was a separate article on the TMSS of functional perovskite published by Li et al.[62] One specific review was published on the synthesis of $BaTiO_3$ NPs using several techniques including the MSS.[178] We have tabulated various perovskite nanomaterials synthesized by the MSS along with the salt used, MOT, and particle characteristics in Table S4.

$BaTiO_3$ is one of the most important ferroelectric materials.[179−185] Designing $BaTiO_3$ nanostructures with well-defined morphologies has been fully explored for its piezoelectric characteristics.[186] There have been a lot of recent reports on this using various wet chemical methods.[187−190] As listed in Table S4, the MSS has been used to synthesize $BaTiO_3$ nanostructures in the form of nanospheres, nanocubes, nanowire, nanoparticles, nanorods, etc.

In particular, TMSS based on the transformation of localized solid materials via insertion, exchange, or deletion of a single atom is one of the well-known strategies among many others for controlling the shape of materials. $BaTiO_3$ nanorods were synthesized by the TMSS using monoclinic $BaTi_2O_5$ nanorods as a template.[77] The morphological change in the TMSS synthesized $BaTiO_3$ nanorods at different temperatures could be easily seen from the SEM images (Figure 7a−f). Specifically, the $BaTi_2O_5$ nanorod shape was intact and well retained up to 700 °C. Beyond that temperature, the $BaTi_2O_5$ rods ruptured into smaller nanorods consisting of $BaTiO_3$ NPs. At 1000 °C, most of the $BaTiO_3$ nanorods transformed into $BaTiO_3$ NPs. This thermally induced conversion of monoclinic $BaTi_2O_5$ nanorods into $BaTiO_3$ nanorods is schematically shown in Figure 7g.

In another work, $BaTiO_3$ NPs and nanorods were synthesized using TiO_2 spheres and $BaTi_2O_5$ rods as precursors (Figure S3).[191] The postulated mechanisms for the formation of the $BaTiO_3$ NPs were dissolution−precipitation (D-P) whereas that of the $BaTiO_3$ nanorods was dissolution−diffusion (D-D) also known as the TMSS.

$BaTiO_3$ supercages were synthesized via the reaction between TiO_2 and hydrated molten salt (HMS) of $Ba(OH)_2{\cdot}8H_2O$ by the MSS for 15 h at temperatures as low as 180 °C (Figure 8).[192] The HMS acted uniquely as the solvent and reactant which ensured efficient interaction among the precursor particles compared to other convention solvents such as water or organic liquid. Hence, the novel phase and structure of perovskite $BaTiO_3$ supercages can be stabilized.

4.2.2. ABO_2-Type Delaffosite. The structure of ABO_2-type delaffosite oxides comprises of edge share distorted BO_6 octahedra arranged in alternate layers whereas A cation is oriented in 2D closed pack array of O−A−O in dumbbell shape and oxygen is tetrahedrally coordinates with one monovalent A^+ cation and three trivalent B^{3+} cations. Delaffosite NPs have been synthesized by hydrothermal means,[193−196] flash autocombustion,[197] chemical deposition,[198] a glycine−nitrate process,[199] an oxygen plasma enhanced reactive evaporation technique,[200] sol−gel,[201] and coprecipitation methods.[202] The MSS has been used as an

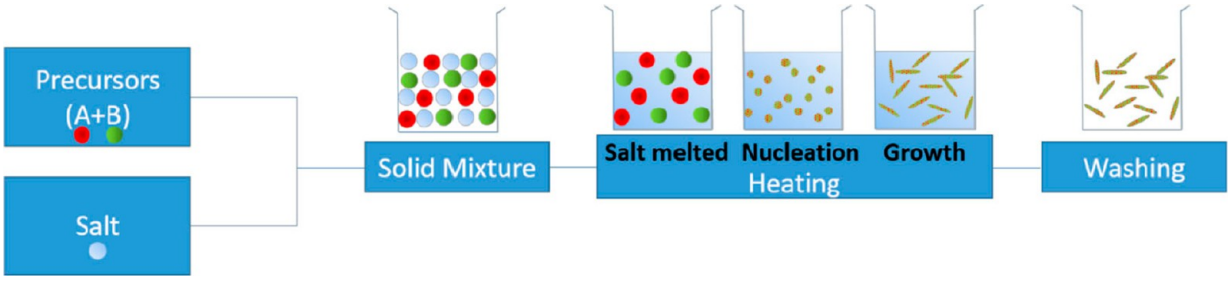

Figure 6. General MSS of complex ternary metal oxide nanomaterials.[65] Copyright 2016. Reproduced with permission from Springer Nature.

https://dx.doi.org/10.1021/acs.jpcc.0c10981
J. Phys. Chem. C XXXX, XXX, XXX−XXX

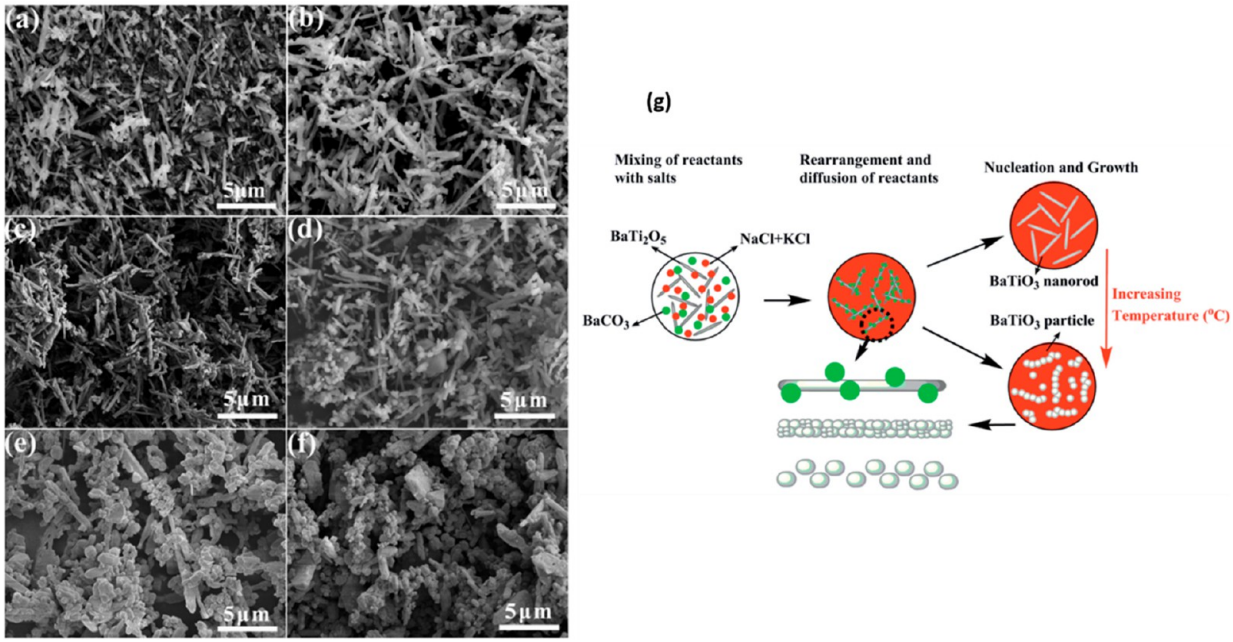

Figure 7. $BaTiO_3$ nanorods prepared by the TMSS method: SEM images of the samples synthesized at different temperatures: (a) 600, (b) 650, (c) 700, (d) 800, (e) 900, and (f) 1000 °C. (g) Proposed mechanism.[77] Copyright 2017. Reproduced with permission from the Royal Society of Chemistry.

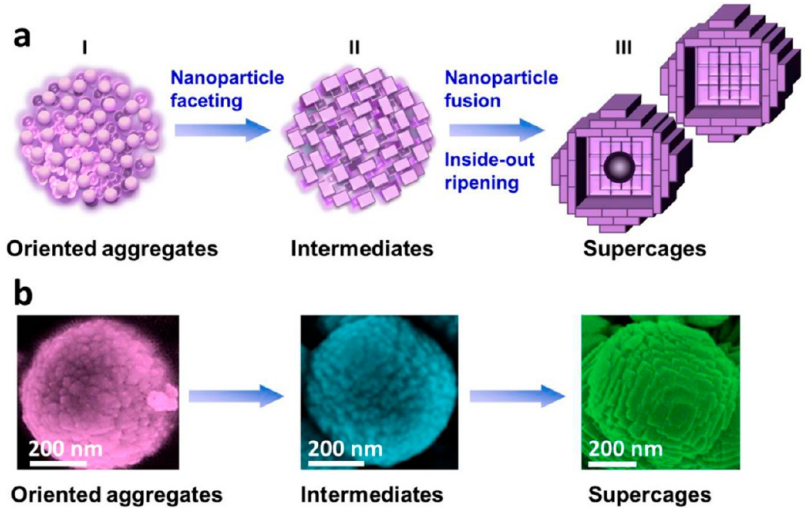

Figure 8. $BaTiO_3$ supercages: (a) Schematic showing the morphostructural transition process and (b) the corresponding SEM images.[192] Copyright 2015. Reproduced with permission from the American Chemical Society.

easy and green method for obtaining delaffosite nanomaterials.

Santra et al. demonstrated the MSS for $CuBO_2$ nanorods using KCl molten salt at 800 °C (Figures S4 and 9).[146] With increasing MSS processing time from 30 min to 60 min and then to 180 min, the number of microrods that were composed of nanorods increased. Specifically, when the MSS processing time was 30 min, the formed $CuBO_2$ nanorods were attached with small and irregular particles of primary $CuBO_2$ nanocrystals which fail to convert into nanorods due to the short processing time. When the processing time was raised to 60 min, these primary attached $CuBO_2$ NPs grew into nanorods and became detached from the host bundle surface, leading to the reduction of roughness on the surface of the nanorods. After 60 min of MSS processing time, some of the remnant NPs were still lying on the surface of the $CuBO_2$ nanorods but gradually converted into small nanorods when the MSS processing time was raised to 180 min. These small nanorods formed nanobundles and became detached from the previous host bundle to reduce surface energy. Finally, all nanorods were highly bundled and all the precursors were transformed into the $CuBO_2$ nanorods (and bundles).

4.2.3. AB_2O_4-Type Spinels. AB_2O_4-type spinel compounds have two variants: normal and inverse spinel structures differing in the distributions of divalent A and trivalent B cations at tetrahedral (T_d) and octahedral (O_h) sites. There has been continuous search for low temperature, easy to perform and mild approach to synthesize spinels. However, it is still a major challenge to synthesize uniform spinel NPs

https://dx.doi.org/10.1021/acs.jpcc.0c10981
J. Phys. Chem. C XXXX, XXX, XXX−XXX

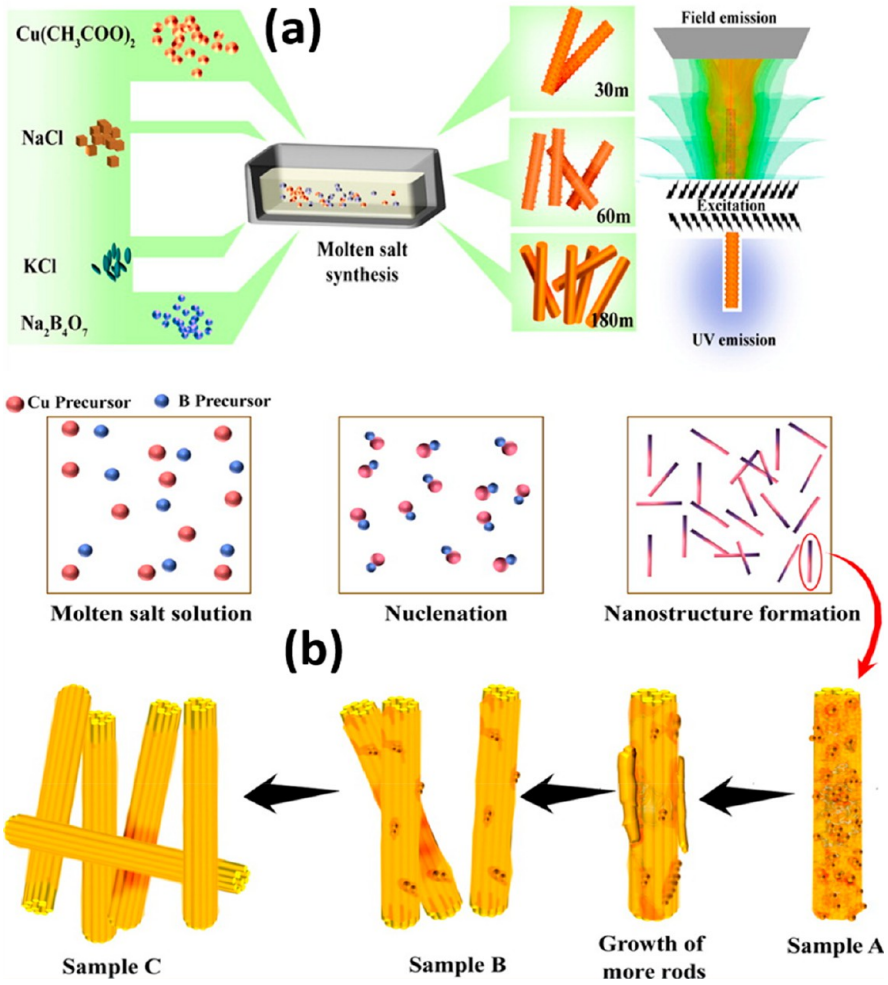

Figure 9. (a) Schematic of the synthesis process and (b) the proposed growth mechanism of the MSS synthesis of $CuBO_2$ nanorods.[146] Copyright 2015. Reproduced with permission from the American Chemical Society.

under nonharsh environment and through environmentally friendly approach. Table S5 lists some recent additions of spinel nanomaterials by the MSS.

Ferrites are important spinels.[72,203−206] Other than TMSS, AMSS is another addition to the MSS. AMSS leads to crystal nucleation and growth, especially those with well-defined facets and commonly seen in nature, by removing volatile component or aerosol droplet cooling.[74] Fu et al. successfully synthesized $CoFe_2O_4$ nanoplates (Figure 10, parts A−C and G) and octahedra (Figure 10, parts D−F and H) using the AMSS with sodium carbonate and sodium molybdate as the molten salts, respectively.[72] They combined topochemical conversion with the AMSS via generating layered double hydroxide (LDH) to stabilize the $CoFe_2O_4$ nanoplates and octahedra. Without adding molten salt, $CoFe_2O_4$ microspheres were synthesized under the same conditions.

On the other hand, Huang et al. synthesized $NiFe_2O_4$ nanoplates containing nanosized building blocks using the MSS with NaCl-KCl molten salt.[203] They tuned the morphology of the synthesized $NiFe_2O_4$ nanoplates by modulating the concentration of the molten salt (Figure S5). They ascribed the effect of the molten salt on the aspect ratio of nanoplates and morphology of nanosized building blocks. They also postulated that lower salt concentration led to larger and thicker nano-octahedron-like building blocks whereas higher salt concentration gave smaller and thinner nanosheet building blocks.

4.2.4. $A_2B_2O_7$-Type Pyrochlores. Because of unique properties of $A_2B_2O_7$-type pyrochlore materials,[160,161] they have displayed various technological applications.[7,19,160,161] Doping pyrochlore materials can also lead to interesting optical properties, order−disorder phase transitions, catalytic properties, magnetic properties, etc.[7,207−211] While Wang et al. published a brief review on various synthesis methods for $A_2B_2O_7$ powders and ceramics,[212] some recent additions of $A_2B_2O_7$-type pyrochlore microcrystals and nanocrystals by the MSS are tabulated in Table S6.

In recent years, the MSS method has been regarded as an effective and convenient method to synthesize pyrochlore NPs at relatively low temperature with high level of monodispersity. Our group has developed a kinetically modified MSS procedure to synthesize $A_2B_2O_7$ NPs with lanthanide ion doping and core−shell structural modifications employing single source precursors.[213] Moreover, to fine-tune their luminescence properties, we have adjusted the processing parameters, such as coprecipitation pH, processing duration, synthesis temperature, postsynthesis annealing, etc.[214−217]

Recently, we highlighted the advantages of the MSS over direct calcination in terms of synthesizing $La_2Hf_2O_7$ and $Pr_2Hf_2O_7$ NPs at 650 °C (Figure S6).[218] Direct calcination

https://dx.doi.org/10.1021/acs.jpcc.0c10981
J. Phys. Chem. C XXXX, XXX, XXX−XXX

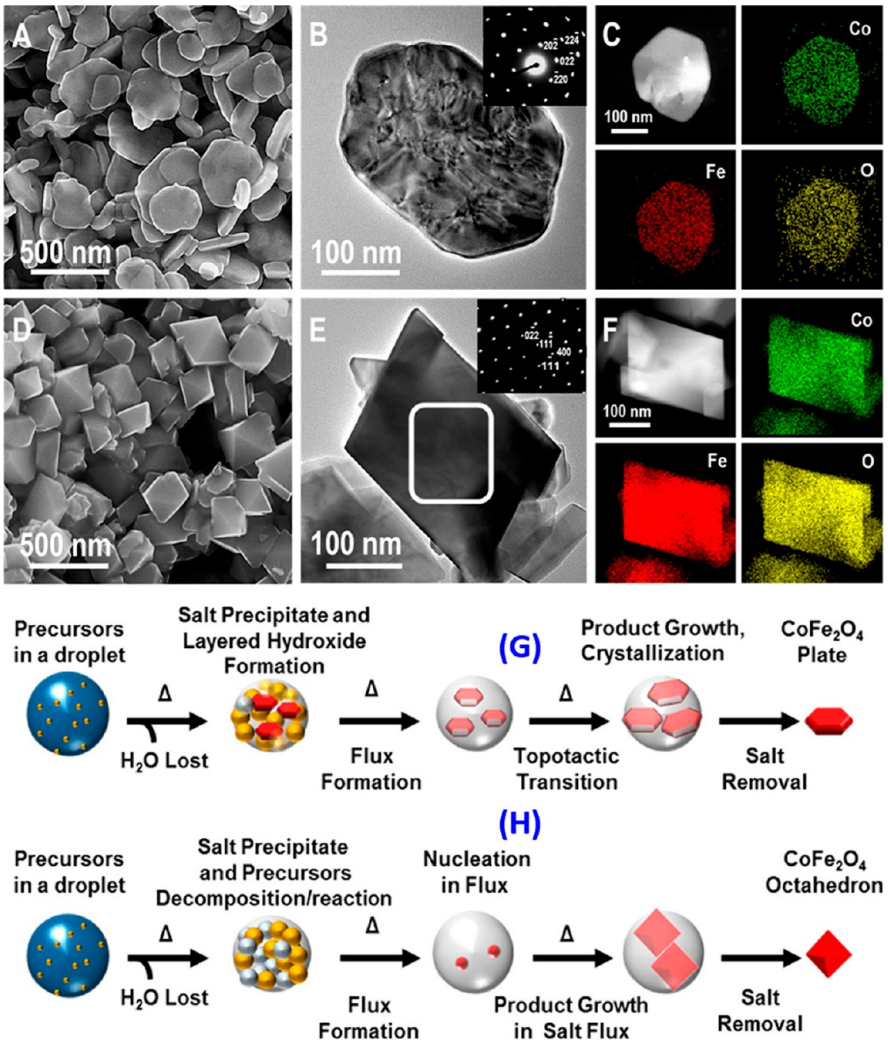

Figure 10. (A and D) SEM images, (B and E) TEM images with insets of SAED patterns, and (C and F) STEM images along with elemental mapping of $CoFe_2O_4$ nanoplates and octahedron, respectively. Schematics for the formation of (G) $CoFe_2O_4$ nanoplate via topotactic transition and (H) $CoFe_2O_4$ octahedra via direct melt crystallization.[72] Copyright 2015. Reproduced with permission from the American Chemical Society.

can synthesize pyrochlore phase but needs a higher temperature while the obtained particles are not in a nanosized domain rather than in a micrometer sized one (Figure S6). The $La_2Hf_2O_7$ NPs by the MSS were mostly spherical and, under certain conditions, had an average diameter of ∼10−12 nm (Figure S7).[217] The Fourier transformed image illustrated the lattice planes in two different sized NPs, showing interplanar spacings of approximately 3.125 and 3.202 Å, which correspond to the (222) and (311) planes of ordered pyrochlore $La_2Hf_2O_7$, respectively.

4.2.5. Other Multinary Oxides. Several other complexes multinary oxides (CMOs) which have been synthesized by the MSS in nanosized dimensions are tabulated in Table S7. For example, ligand-free and high crystalline $La_{1-x}Sr_xMnO_3$ (LSMO) nanocubes with a size of ∼20 nm and extremely low defect density (Figure 11) were synthesized by the MSS in gram scale by N'Goc et al.[219] Because of the highly oxidizing nature of molten salt KNO_3, manganese could be stabilized in a high oxidation state of around 3.33 in the first two layers of the LSMO nanocubes.[220]

Multicationic mesostructures have also been stabilized using the MSS.[221] For example, the $Sr_4Mn_3O_{10}$ platelet at the mesoscale with basal face has dimension of hundreds of nanometers with thickness in the range of 20−100 nm was synthesized at 600 °C using $Sr(OH)_2$ as the molten salt (Figure S8a). Micro-/nanosized Ta-doped LLZO ($Li_{6.4}La_3Zr_{1.4}Ta_{0.6}O_{12}$, LLZTO) was synthesized using the MSS in three different kinds of salts, i.e. LiCl-KCl (X), LiCl-LiOH (Y), and highly basic $LiNO_3$−LiOH-Li_2O (Z).[222] The salt X/Y led to the LLZTO powder with larger particles compared to salt Z (Figure S8b,c). Moreover, as the basicity of the molten salt increased, the formation temperature needed for synthesizing the LLZTO garnet decreased (Figure S8d).

4.2.6. Other Technologically Important Oxides: Metal Phosphates, Vanadates, Tungstates, and Molybdates. Some metal phosphate nanomaterials synthesized by the MSS include Eu^{3+}-doped $LaPO_4$ and $Na_3Bi(PO_4)_2$.[223,224] Huang et al. synthesized quasi-hexagonal $LaPO_4$ NPs with a mean size of 30 nm at temperatures as low as 160 °C in the molten salt of NH_4NO_3.[223] The synthesized NPs were highly monodispersed and nanocrystalline in nature with well-

https://dx.doi.org/10.1021/acs.jpcc.0c10981
J. Phys. Chem. C XXXX, XXX, XXX−XXX

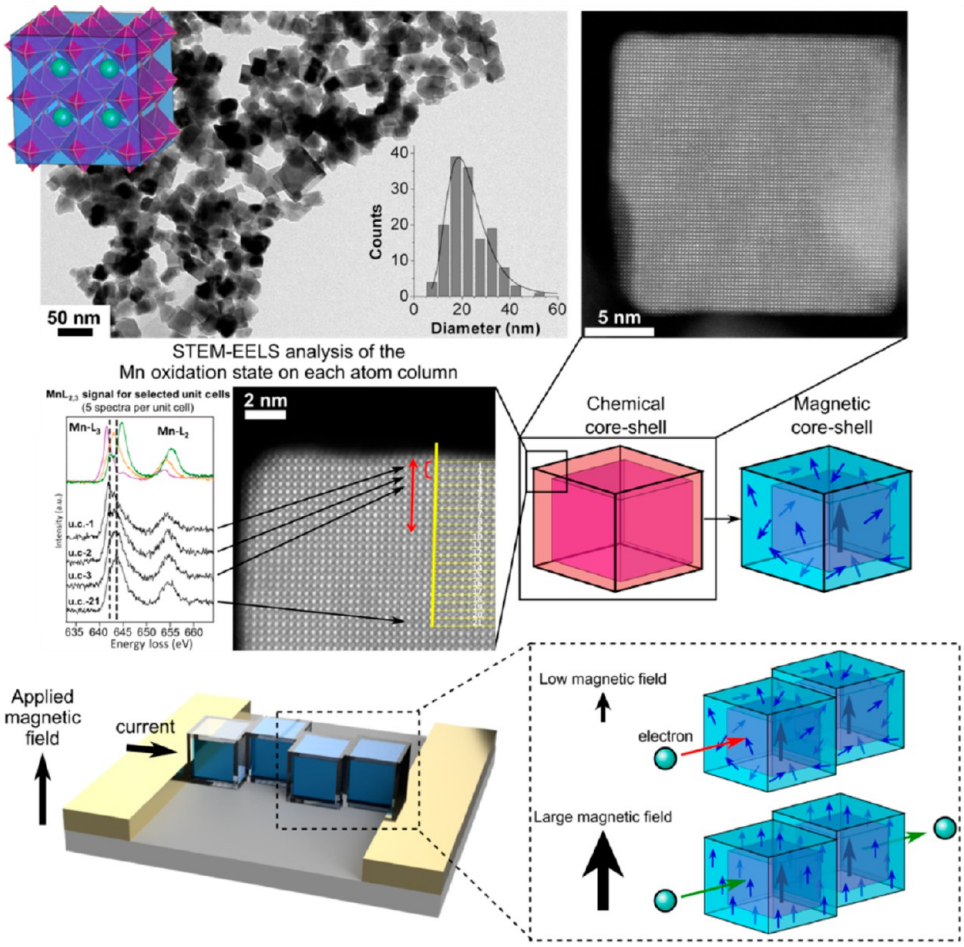

Figure 11. LSMO nanocubes synthesized by the MSS in gram scale.[220] Copyright 2018. Reproduced with permission from the American Chemical Society.

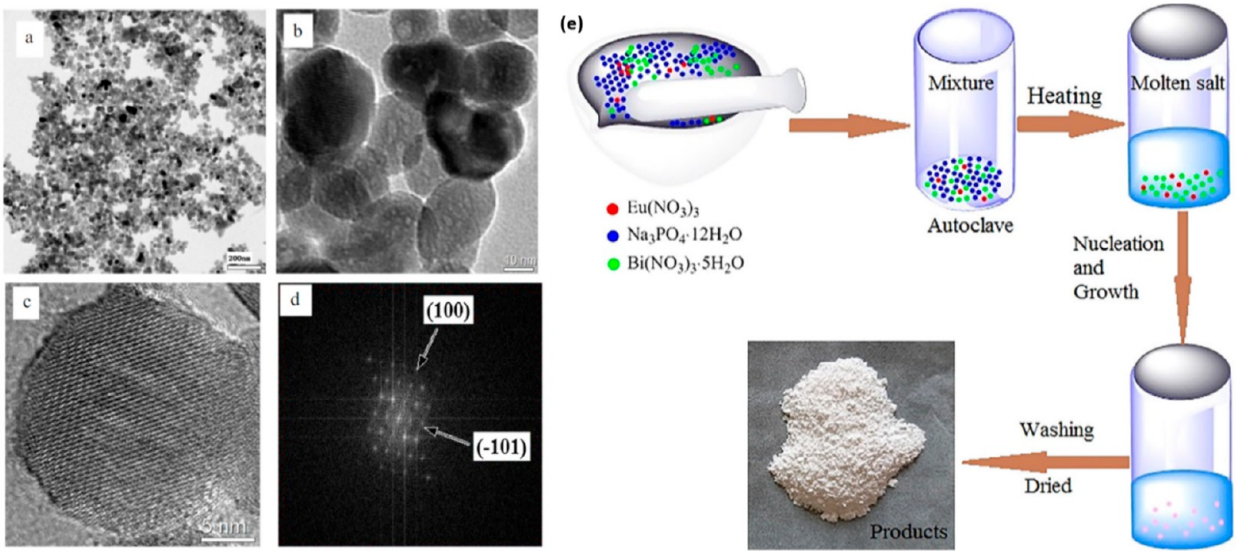

Figure 12. (a, b) TEM images, (c) HRTEM image, and (d) SAED pattern of the $LaPO_4$:Eu^{3+} NPs formed by the MSS.[223] Copyright 2015. Reproduced with permission from Elsevier. (e) Schematic of the MSS for $Na_3Bi(PO_4)_2$:Eu^{3+}NPs.[224] Copyright 2019. Reproduced with permission from John Wiley and Sons.

defined facets (Figure 12). Wang et al. synthesized $Na_3Bi(PO_4)_2$:Eu^{3+} NPs using intrinsically formed $Na_3PO_4{\cdot}12H_2O$ as the molten salt to ensure a conducive chemical environment with high thermal conductivity and mass transfer coefficient for the formation of uniform and homogeneous NPs.[224]

Golyeva et al. synthesized YVO_4:Eu^{3+} nanomaterials in KCl molten salt.[225] Alsheri et al. recently synthesized $ZnWO_4$ and

https://dx.doi.org/10.1021/acs.jpcc.0c10981
J. Phys. Chem. C XXXX, XXX, XXX−XXX

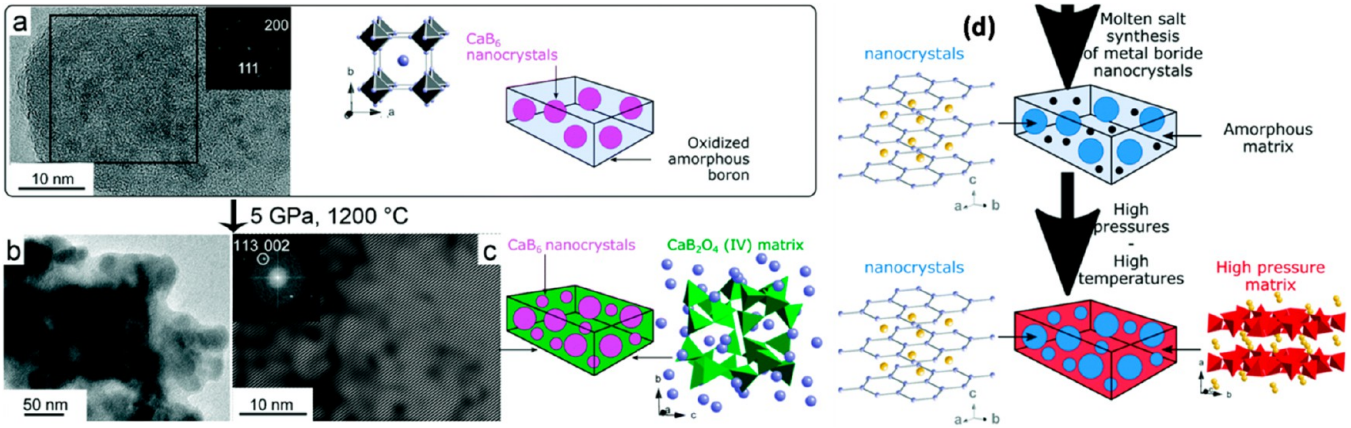

Figure 13. TEM images of the MSS synthesized (a) CaB_6 and (b, c) CaB_2O_4 nanocrystals which were generated at HT-HP. (d) Schematic of the HT-HP aided MSS transformation from CaB_6 to CaB_2O_4.[246] Copyright 2018. Reproduced with permission from the Royal Society of Chemistry.

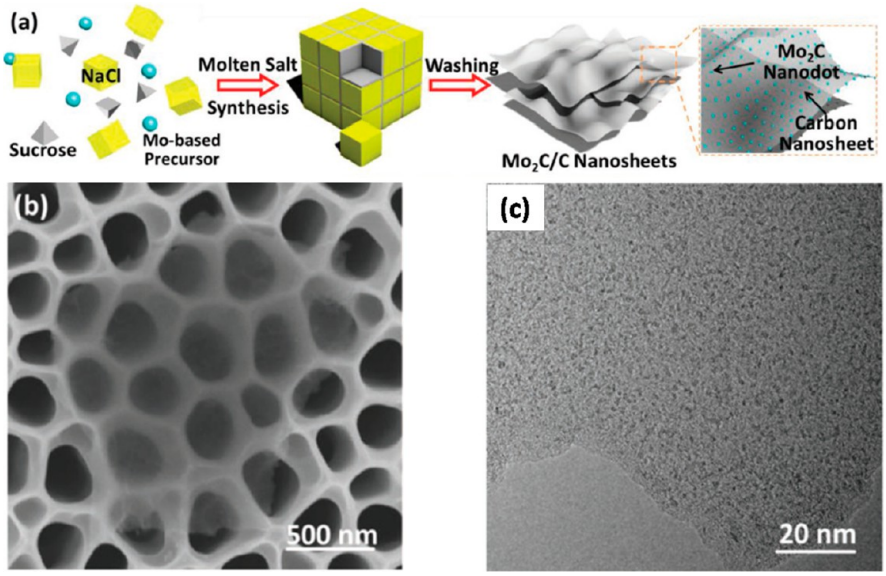

Figure 14. Mo_2C nanodots included in carbon nanosheet synthesized via the MSS method: (a) schematic of the proposed growth mechanism, (b) SEM image, and (c) TEM image.[260] Copyright 2018. Reproduced with permission from John Wiley and Sons.

$NiWO_4$ nanobricks using the MSS.[226,227] $NiWO_4$ nanobricks with a diameter of ∼20 nm and a high surface area of ∼25 m^2/g were synthesized in the molten salt of $NaNO_3$ + KNO_3 (Figure S9). In addition, there were a few more reports on the MSS synthesis of $NiWO_4$ nanopowder, $ZnWO_4$ nanopowder, and cube-shaped $CoWO_4$ NPs (∼30 nm).[228−231] In another report, Bi_2WO_6 nanosheets synthesized by the MSS showed much higher crystallinity, light-harvesting capability and sorption capacity compared to those synthesized hydrothermally.[232]

The MSS has also been utilized judiciously to synthesize different variants of bismuth molybdates including Bi_2MoO_6, $Bi_6Mo_2O_{15}$, Bi_4MoO_9, and $Bi_{14}MoO_{14}$ employing $NaNO_3$+KNO_3 as the molten salt.[233] Interestingly these different molybdates were formed by altering the ratio of the Bi/Mo precursors at the MOT of 500 °C. Specifically, the Bi_2MoO_6 stabilized in 2D microsheets with a thickness in the range of 20−50 nm. The $Bi_6Mo_2O_{15}$ assumed in a 1D shape of nanowires in the diameter range of 30−150 nm. On the other hand, the Bi_4MoO_9 and $Bi_{14}MoO_{24}$ exhibited irregular 3D bulk-shaped nanostructures.

5. OTHER NANOMATERIALS SYNTHESIZED BY THE MSS METHOD

5.1. Metal Borides. Metal borides have constituted several technological applications, while there is relatively less work being carried out on them mainly due to their synthesis challenges.[234,235] Often they are synthesized by SSR or reducing metal oxides or salts with boron compounds in molten metals and fused salt electrolysis.[236−238] These techniques lead to poor quality powders with nondefined size and shape as well as a low level of crystallinity.[239,240] Nanostructured metal borides were mostly synthesized by CVD, ball-milling, arc plasma, etc. These techniques require sophisticated instruments, have toxic remnants, and are difficult to operate in normal laboratories.[241] Their synthesis in nanodomains in particular is extremely important owing to several unique properties associated with the enhancement of T_m, chemical stability, hardness and wear resistance, magnetic behavior, and biocompatibility compared to their bulk counterpart.[242−244] The MSS recently has been found to be one of the most sought out options to synthesize metal

https://dx.doi.org/10.1021/acs.jpcc.0c10981
J. Phys. Chem. C XXXX, XXX, XXX−XXX

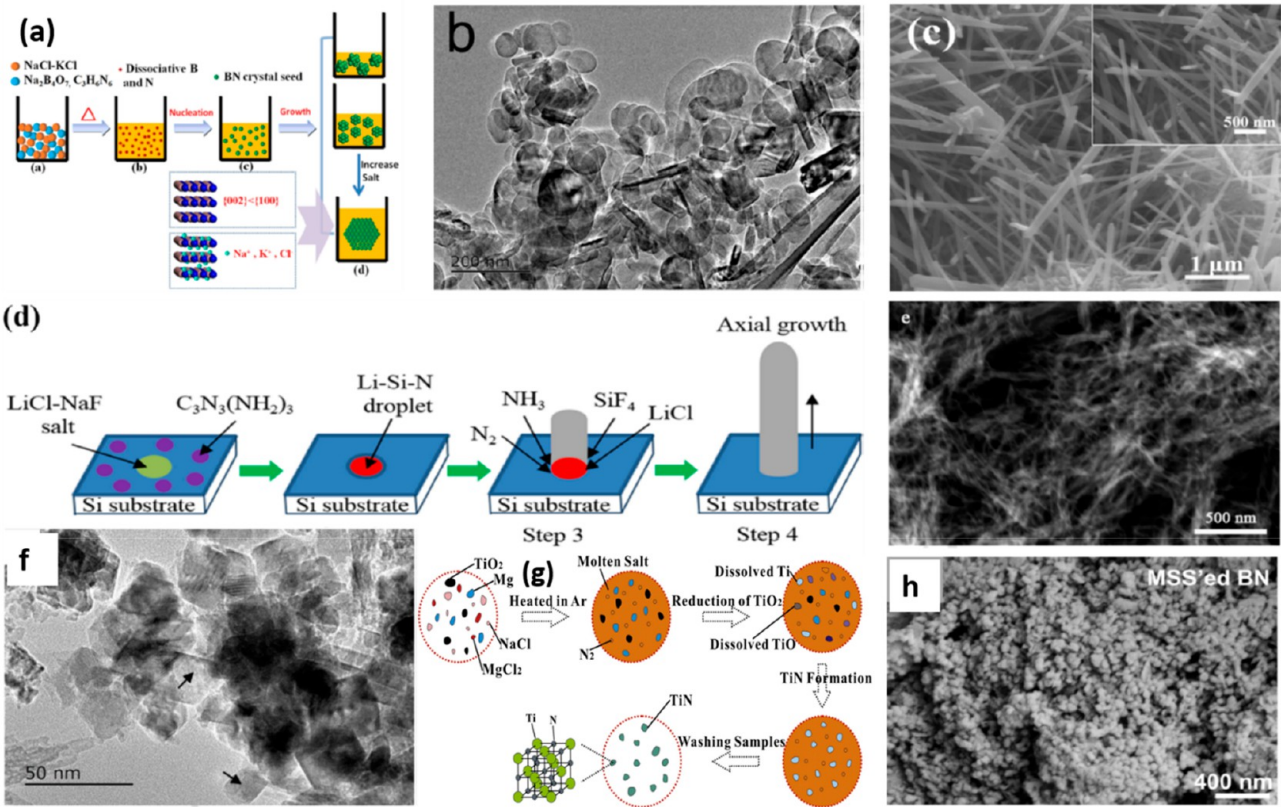

Figure 15. (a) Proposed growth mechanism and (b) TEM image of the BN nanosheets synthesized by the MSS.[267] Copyright 2019. Reproduced with permission from Elsevier. (c) TEM and (d) proposed growth mechanism of the $LiSi_2N_3$ nanobelts by the MSS.[264] Copyright 2016. Reproduced with permission from the Royal Society of Chemistry. (e) TEM image of the seaweed-like CN nanostructure synthesized by the MSS.[268] Copyright 2016. Reproduced with permission from Elsevier. (f) TEM and (g) plausible reaction mechanism of the TiN nanocube synthesized by the MSS.[263] Copyright 2017. Reproduced with permission from Elsevier. (h) TEM image of the BN nanosphere synthesized by the MSS.[266] Copyright 2019. Reproduced with permission from Elsevier.

borides. We have tabulated the metal boride nanostructures synthesized by the MSS in the past 6 years in Table S8.

As a specific example, Jothi et al. recently reported a simple, facile, and general approach for synthesis of various nanocrystalline TMBs by taking advantages of the redox chemistry of $Sn/SnCl_2$, the volatility and recrystallization of $SnCl_2$ at the synthesis conditions, and the immiscibility of tin with boron.[245] Moreover, Grosjean et al. synthesized CaB_6 nanocrystals of ∼15 nm using the MSS approach (Figure 13a).[246] When such nanocrystals were exposed to high temperature and high pressure (HT-HP, 5 GPa, 1200 °C), they grew slightly only up to 30 nm but crystallized into the new phase of CaB_2O_4 (Figure 13b,c). Moreover, Grosjean et al. synthesized β-HfB_2O_5 and CaB_2O_4 nanocomposites by heating the ambient pressure molten salt synthesized borides HfB_2 and CaB_6 nanocrystals at higher pressure (Figure 13d).[246]

5.2. Metal Carbides. Many transition metal carbides (TMCs) show superior electrical, mechanical, and optical properties.[247−249] Designing nanostructured TMCs with high crystallinity, well-defined size/shape and accessible surface remains a huge challenge to achieve, particularly at low temperature, as concisely reviewed by Rasaki et al.[250,251] Luc et al. summarized the synthesis of nanoporous metal carbides in 2016.[252] The MSS method is one of the most viable options to achieve uniform crystalline nanostructured metal carbides with well-defined size/shape and low defect density as compiled in Table S9.

Leonard et al. synthesized several TMC nanowires such as Nb_4C_3, Cr_3C_2, TaC, and WC by the MSS (Figure S9).[253] The MSS was also successful to synthesize complex nanostructured metal carbides such as Ti_3AlC_2 and $(Ta_{0.25}Nb_{0.25}Ti_{0.25}V_{0.25})C$.[254−258] The as-synthesized nanostructured Ti_3AlC_2 was converted into Ti_3C_2 by etching in hydrofluoric acid.[256,258]

Moreover, carbide-derived carbon could also be successfully synthesized using the MSS method as a new class of porous materials.[259] Cheng et al. incorporated Mo_2C nanodots in carbon nanosheet via the MSS (Figure 14).[260]

5.3. Nitrides and Oxynitrides. Nitrides possess extremely high lattice energy and refractory nature.[73,250,261−271] The design of blue-emitting GaN endowed three Japanese scientists with the Nobel Prize for Physics in 2014.

As reviewed by Rasaki et al., many metal nitrides have been synthesized by the MSS method.[250] For example, there were recent reports on the synthesis of water dispersible polymeric carbon nitride nanoseaweeds from NaCl−KCl molten salt,[268] $LiSi_2N_3$ nanobelts from NaCl−NaF molten salt,[264] nanosheet, nanosphere, and nanoplates of boron nitride from NaCl−KCl,[266,267,270] titanium nitride NPs from $MgCl_2$−NaCl flux,[262,263] and VN nanopowder from KCl−KF flux,[265] etc. Parts a and b of Figure 15 show the mechanism and the TEM image of the BN nanosheets synthesized by the MSS method.[267] $LiSi_2N_3$ nanobelts were successfully synthesized via the molten salt nitridation employing Si and melamine as precursors and LiCl−NaF as the molten salt at 1200 °C,

https://dx.doi.org/10.1021/acs.jpcc.0c10981
J. Phys. Chem. C XXXX, XXX, XXX−XXX

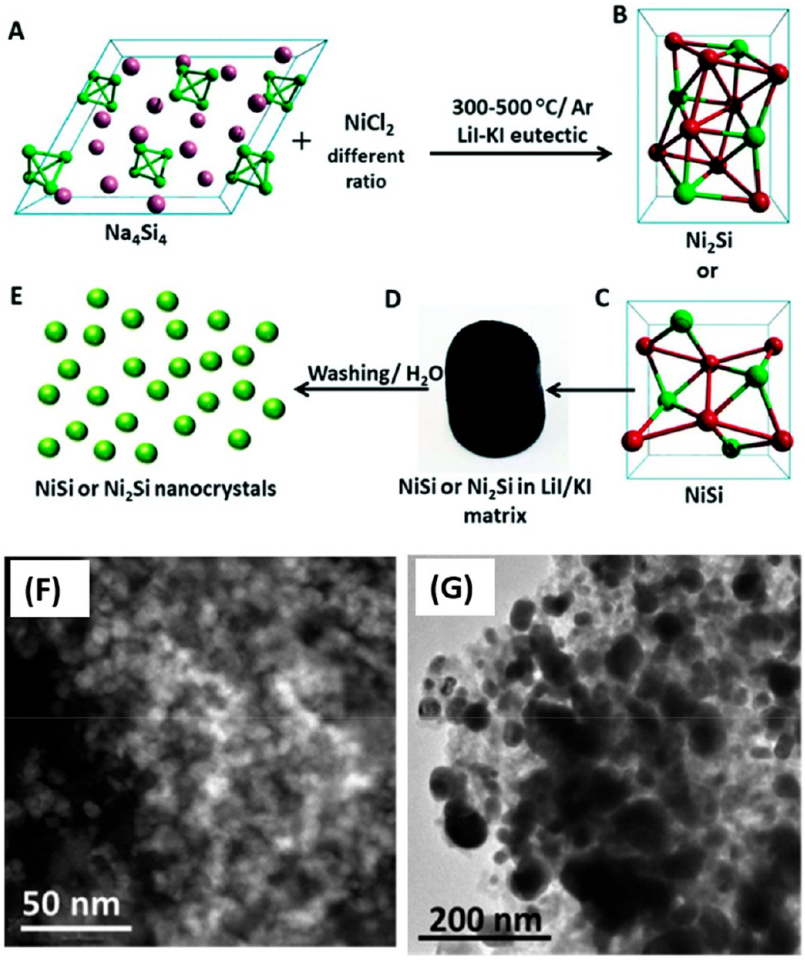

Figure 16. (A–E) Schematic of the MSS of NiSi and Ni_2Si nanocrystals using LiI–KI eutectic. (F and G) HAADF-STEM images of the formed Ni_2Si and NiSi nanocrystal, respectively.[285] Copyright 2020. Reproduced with permission from the Royal Society of Chemistry.

which was 200 °C lower than that for conventional SSR (Figures 15c,d).[264] Unique and novel seaweed-like CN nanostructure (Figure 15e) was achieved by the MSS method using melamine as precursor and NaCl–KCl as the molten salt.[268] TiN nanocubes could also be synthesized using the MSS (Figure 15, parts f and g).[263] The MSS was also used to obtain BN NPs (Figure 15h).[266] Chen et al. reported on the rhombohedral BN nanoflakes by the MSS using NaCl–KCl flux.[261] One can also synthesized doped nitrides via the MSS as demonstrated by boron-doped C_3N_4 using mixed KCl–NaCl–LiCl salt.[272]

The MSS was also explored to synthesize carbon nitride quantum dots in the size domain of 2.5 nm (Figures S11a,b).[269] The uniqueness of the AMSS was exploited to synthesize Ta_3N_5 nanoplates in different shapes and sizes (Figure S11c).[73] These authors further investigated the temperature effect on the morphology and crystal structure of rhombohedral BN synthesized by the MSS. Furthermore, there have been a few reports on the MSS of oxynitride nanomaterials such as boron carbon oxynitride nanosheets, oxynitride nanotubes, and $LaTaON_2$ nanocubes.[273−275]

5.4. Fluorides. Fluorides are considered excellent luminescence hosts for solid-state phosphors and upconversion applications attributed to the low phonon energy leading to high luminescence efficiency. While their nanostructures have been synthesized mainly by colloidal method, the MSS has becoming a popular alternative. For example, Pederov et al. synthesized CaF_2, SrF_2, REF_3, and $NaREF_4$ (RE = La, Ce, Y) from the corresponding metal nitrates dissolved in molten $NaNO_3$ with NaF as fluorinating agent (Figure S12a-d).[276,277] NaF is considered the best fluorinating agent for the MSS of fluorides owing to its decent solubility in water and low melting point (994 °C).[276] PbF_2 was used the solvent for the synthesis of single crystals of K_2NaGaF_6 and Rb_2KGaF_6.[278]

Huang et al. synthesized hexagonal $NaBiYF_4$:Er^{3+}/Yb^{3+} micro-/nanocrystals employing the MSS in NH_4NO_3 flux along the investigation of the effect of flux amount, reaction time and temperature on the structure and morphology.[279] The same group extensively studied the synthesis of LnF_3 and $NaLnF_4$ NPs with almost all lanthanides (Ln = La, Ce, Pr, Nd, Sm, Eu, Gd, Tb, Dy, Ho, Y, Tm, Yb, and Lu) by the MSS and noticed that the size of lanthanide ions played an important role in the phase stability and morphology of the formed particles.[280]

As one of the most efficient upconversion materials for a wide range of applications, $NaYF_4$:Yb^{3+},Er^{3+} was synthesized in nano-/micro domains using the MSS.[281] For example, Fedorov et al. synthesized inorganic fluorides using two different kinds of molten media: salts and ionic liquids.[282] Their extensive investigation indicated that the size of fluoride particles could be reduced from few millimeters to as low as 30 nm by lowering the MOT from 800 to 150 °C. Based on their investigations with two different molten media, they postulated that non-agglomerated fluoride NPs

https://dx.doi.org/10.1021/acs.jpcc.0c10981
J. Phys. Chem. C XXXX, XXX, XXX−XXX

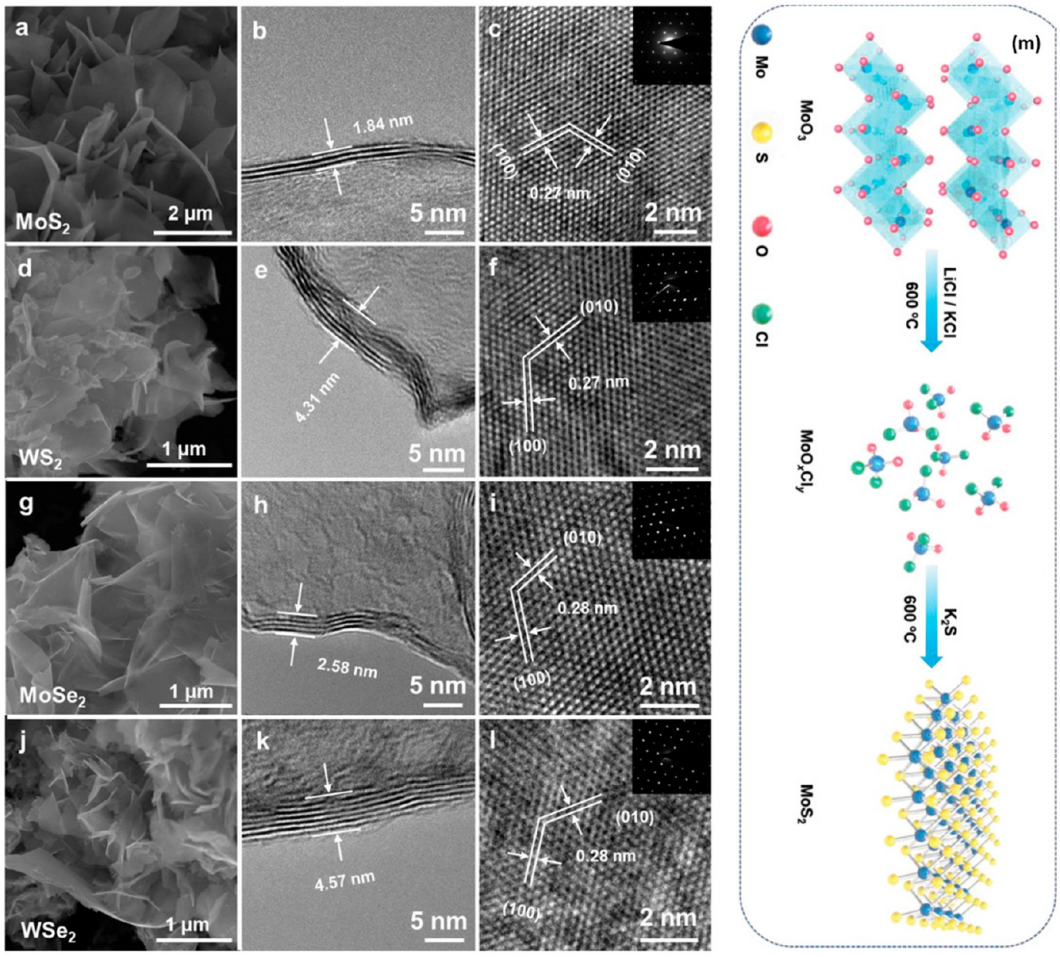

Figure 17. Nanosheets of several TMCs: (a−c) MoS_2, (d−f) WS_2, (g−i) $MoSe_2$, and (j−l) WSe_2 with their SEM, HRTEM of the edge, and HRTEM images, respectively. (m) Schematic of the MSS of MoS_2 nanosheets employing LiCl/KCl salt.[295] Copyright 2019. Reproduced with permission from John Wiley and Sons.

could form in ionic liquid whereas equilibrium phases of $NaYF_4$ could be synthesized via the MSS at 300 °C.

5.5. Silicides. Transition metal silicides (TMSs) have also fetched a lot of attention.[283] Specifically, some of silicides such as $MgSi_2$ NPs are proposed as deoxygenating agents for cancer therapy.[284] Kumar et al. demonstrated the MSS of NiSi and Ni_2Si nanocrystals using LiI−KI eutectic salt by an exchange reaction between different molar ratios of $NiCl_2$ and Zintl solid Na_4Si_4 (Figure 16).[285] The formed Na_2Si and NiSi nanocrystals were initially embedded inside the LiI−KI eutectic salt before being washed with suitable solvents, acidic water in this case. There is another work on the MSS of highly complex high entropy silicide nanopowder $(Nb_{0.25}Ta_{0.25}Ti_{0.25}Hf_{0.25})Si_2$.[286] Godfroy et al. synthesized $CrSi_2$ NPs using the reaction between $CrCl_3$ and Si in the presence of NaCl−LiCl salt to reduce the particle size.[287] As an important functional material, $MoSi_2$ NPs were successfully synthesized by Nersisyan et al. using the NaF molten salt.[288] Some research groups also explored the MSS in the NaCl−$CaCl_2$ molten salt to synthesize ZrSi/ZrC nanocomposites.[289] It could also be possible to synthesize silicide coating on metal substrate by electrodeposition in molten salt.[290,291]

5.6. Chalcogenides. Transition metal chalcogenides (TMCs) show exceptional physical and chemical properties which lead to several applications.[292−299] As reviewed by Kim et al. on the synthesis and application of nanostructured metal chalcogenides,[296] there have been quite a few reports on the MSS of nanostructured TMCs such as MoS_2, WS_2, $MoSe_2$, WSe_2, Mo_2S_3, Cu_2ZnSnS_4, $CuInS_2$, etc.[293−295,299] The efficacy of this generalizable synthesis approach could be seen from its synthesis of MX_2 (M = Mo, W and X = S, Se) nanosheets (Figure 17).

Zhou et al. synthesized novel urchin-like Mo_2S_3 nanostructures by the MSS (Figure 18a−c).[299] Wang et al. reported a MSS assisted chemical vapor deposition approach to synthesize $MoSe_2$ monolayer.[300] Complex alkali metal-doped Co_9S_8 NPs embedded within N,S codoped mesoporous carbon were successfully synthesized using the MSS strategy.[301] Tan et al. also synthesized large and thin TiS_2 sheets via a gas/molten salt interface reaction and clearly pinpointed that the flux played an extremely important role in stabilizing this interesting and complex chalcogenide material.[302] More specifically, these TiS_2 sheets could be synthesized with flux combinations of KCl/NaCl, KCl/LiCl, and NaCl/$CaCl_2$, but this was not possible with $CaCl_2$ and $ZnCl_2$.

A few more chalcogenides and related materials have also been successfully synthesized by the MSS strategy, such as $Fe(Se_{0.5}Te_{0.5})$ solid pellet, 1D zinc selenophosphates, sulfur-doped silicon, $La_3Fe_{0.5}GeSe_7$, $La_3MnGaSe_7$, $Ce_3Fe_{0.5}SiSe_7$, $Ce_3Mn_{0.5}SiSe_7$, $Sm_3Fe_{0.5}SiSe_7$, $Sm_3Mn_{0.5}GeSe_7$,

https://dx.doi.org/10.1021/acs.jpcc.0c10981
J. Phys. Chem. C XXXX, XXX, XXX−XXX

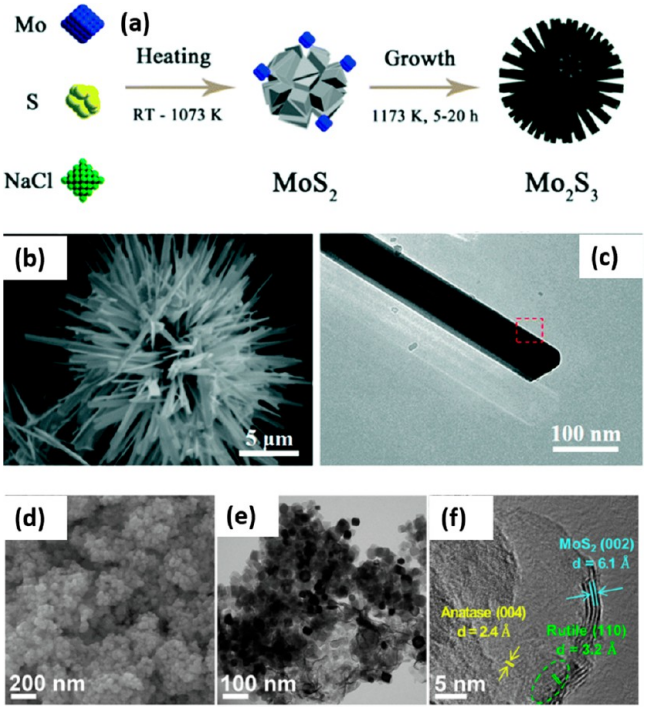

Figure 18. Urchin-like Mo_2S_3: (a) schematic of the MSS mechanism in NaCl, (b) SEM image, and (c) TEM image.[299] Copyright 2018. Reproduced with permission from the Royal Society of Chemistry. The MSS synthesized TiO_2 NPs and MoS_2 (5.0%) nanosheet heterojunction: (d–f) SEM, TEM and HRTEM images, respectively.[308] Copyright 2020. Reproduced with permission from Elsevier.

$Cu_{10}Cd_2Sb_4S_{13}$, etc.[303−307] The MSS has also been employed to prepare chalcogenide-related heterojunctions. For example, Zhong et al. synthesized TiO_2 NP@MoS_2 nanosheet heterojunction using the MSS strategy (Figure 18d–f).[308] Similarly, the MoS_2@CoS_2 heterostructure was achieved using the MSS at very low temperature for hydrogen evolution reaction catalysis.[80]

5.7. Oxyhalides. The MSS has proven to be an efficient approach for achieving complex nanosized M-O-X-type oxyhalides.[309,310] Specifically, oxyhalides such as Bi_4TaO_8Cl, Bi_4NbO_8Cl, and Bi_2NbO_5F have been synthesized by the MSS.[311−313] Using the MSS, Li et al. successfully synthesized Bi_4TaO_8Cl square nanoplates with a regular orthorhombic structure, an edge length of 500 nm, and a thickness of 100 nm (Figure 19).[311] Novel Bi_4NbO_8Cl nanosheets with 3D architecture and layered lanthanide oxychloride were also synthesized using the MSS method.[314,315]

6. CONCLUSIONS AND PERSPECTIVE

In this review article, we discussed different aspects of the MSS for synthesizing high quality nanomaterials for advanced applications. The MSS has opened new avenues for synthesizing novel nanostructured materials and stabilizing unique phases and structures. The advanced MSS techniques such as TMSS, AMSS, and kinetically modified MSS as well as their advantages have also been reviewed in the article.

Bestowed with all its uniqueness, the MSS has been explored for a few other types of advanced materials other than those discussed in the proceeding sections, e.g., two-dimensional metal oxides,[158] stable colloids,[316] and quantum

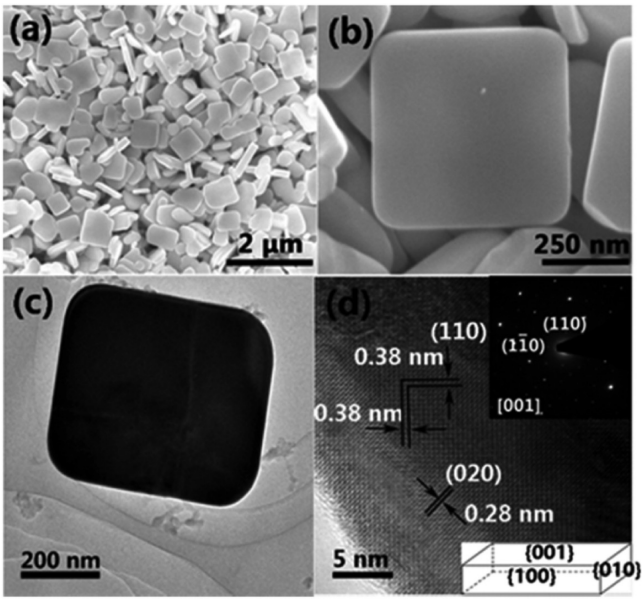

Figure 19. Bi_4TaO_8Cl square nanoplates: (a, b) FESEM images at different magnifications, (c) a TEM image, and (d) a HRTEM image with inset showing SAED pattern.[311] Copyright 2018. Reproduced with permission from the Royal Society of Chemistry.

dots.[317] The perspectives on the MSS for 2D nanomaterials, nanomaterials with polar facets, and intermetallic nanocrystals (INCs) are given below.

The MSS has been exploited in the past few years to synthesize 2D nanosheets using nitrates, hydroxides, and sulfates as molten salts with directly involvement in the reaction with the precursors.[318] It is expected that the MSS will be continuously employed to mass synthesize 2D ion-intercalated metal oxides, hydroxides, carbides, and nitrides (MXenes) among others as the ionized species in the molten salts guide the growth of the 2D structures having a large lateral size with an atomic scale thickness.[319,320]

Crystallites with high-energy surfaces usually exhibit higher reactivity than those with low-energy surfaces. The most effective design approach is using electrostatic interactions to reduce the energy of such planes.[321−324] Endowed with its unique characteristics, the MSS has been explored to design micro- and nanocrystallites with polar surfaces exposed ZnO, MgO, Co_3O_4, and $ZnFe_2O_4$.[324−326] We expect the MSS will be further investigated to synthesize other nanomaterials to keep demonstrating its universality as a polar and high-energy-surface engineering strategy.

Recently exploration has been made to search for intermetallic nanocrystals to expand the property landscape and allow property and performance improvement.[327] While the synthesis of intermetallic nanocrystals has been a huge challenge to materials scientists, the reports on intermetallic nanocrystals of Pt_3Y, Pt_3Sc, Pt_3Lu, Pt_2Na, and Au_2Y, etc. have demonstrated that the MSS is an effective synthesis approach and should be further explored for them.[328,329]

Molten salts and ionic liquids, which in general are composed of simple ionic pairs and large ionic species and are used in high and low temperature ranges, respectively, seem to be going in opposite directions in the plethora of the syntheses of nanomaterials.[330] It can be a boon to ionic liquid researchers if both empirical and theoretical knowledge of molten salt chemistry can be transferred to them or *vice*

https://dx.doi.org/10.1021/acs.jpcc.0c10981
J. Phys. Chem. C XXXX, XXX, XXX−XXX

versa. If ionic liquids are considered as ionic salts, several reaction parameters involving them can be explained efficiently by the analogy of electrostatic interactions.[331] It was found that the dynamics of fused molten salt are strongly influenced by charge and mass distribution of the constituting ions.[332] The same can be extended by following the approach of instantaneous normal-mode analysis to investigate how motional dynamics of ions at different frequencies (translational and rotational) by structure of ions in ionic liquids.[332] Therefore, we expect that what we have learned from the molten salt and ionic liquid synthesis of nanomaterials will catalyze rapid developments in both fields while not suggesting that they can be replaced by each other.

While there have been many reports on the MSS of nanomaterials, their crystal nucleation and growth have not much been probed by *in situ* techniques and operando methods.[333] More efforts need to be invested on establishing systematic correlation between experimental synthesis parameters and thermodynamics and kinetics of molten salt reactions in the future. A quantitative approach to understanding the kinetics of molten salt reactions with reactant species can throw light on the role of synthesis parameters for tuning the size, shape, and composition of synthesized nanomaterials.

Overall, the future of the MSS of nanomaterials is bright to bring nanoscience and nanotechnology up to the next level. Because of its various advantages, the MSS can be one of the most attractive options for the nanomaterials synthesis industry. This generalizable approach can lead to the stabilization of various interesting and challenging metastable phases in nanosized domains as demonstrated by Parija et al. with HfO_2 and V_2O_5.[334] This review provides a timely summary for this unique MSS method in preparing size- and shape-tunable nanomaterials, which provide a rich platform for further studies on their properties and exploration of their application potentials.

■ ASSOCIATED CONTENT

Supporting Information

The Supporting Information is available free of charge at https://pubs.acs.org/doi/10.1021/acs.jpcc.0c10981.

> XRD pattern and TEM images of various binary oxides, TEM images of nanowires, growth mechanisms and SEM images of $BaTiO_3$ nanorods, FESEM images of $CuBO_2$ nanorods, SEM images of the $NiFe_2O_4$ nanoplates, schematic showing the formation of pyrochlore NPs by the MSS, TEM images of the $La_2Hf_2O_7$ NPs, TEM images of the $NiWO_4$ nanobricks, TEM images of the TMCs nanowires, TEM images of the CN quantum dots, Ta_3N_5 nanoplates with different sizes and shapes, SEM images of fluoride particles, advantages and disadvantages of various synthesis methods, melting point and chemical composition of some metal halide and oxosalt systems, and examples of nanostructured binary oxides, perovskites, spinels, pyrochlore, multinary oxides, borides, and carbides (PDF)

■ AUTHOR INFORMATION

Corresponding Author

Yuanbing Mao − *Department of Chemistry, Illinois Institute of Technology, Chicago, Illinois 60616, United States;* orcid.org/0000-0003-2665-6676; Email: ymao17@iit.edu; Fax: +1-312-567-3815

Author

Santosh K. Gupta − *Radiochemistry Division, Bhabha Atomic Research Centre, Trombay, Mumbai 400085, India; Homi Bhabha National Institute, Anushaktinagar, Mumbai 400094, India;* orcid.org/0000-0002-1178-0159

Complete contact information is available at: https://pubs.acs.org/10.1021/acs.jpcc.0c10981

Notes

The authors declare no competing financial interest.

Biographies

Dr. Santosh Kumar Gupta is a Scientific Officer at the Radiochemistry Division, Bhabha Atomic Research Centre, since 2010. He received his B.Sc. degree from Delhi University, M.Sc. degree from the Indian Institute of Technology, Delhi, and Ph.D. degree from the Homi Bhabha National Institute, Mumbai, India. He has been awarded with various international fellowships, such as Indo-US, JSPS, and Fulbright fellowships for postdoctoral studies. He was the recipient of the Department of Atomic Energy Group Achievement and Young Scientist award from the Government of India for 2010 and 2017, respectively. As of today, he has published 156 journal articles with approximately 2900 citations, an h-index of 32 and i-10 index of 82. His area of research encompasses photo-/radio-luminescence of lanthanide and actinides, defect spectroscopy, upconversion of nanoparticles, optical materials for health, energy, and environment, etc.

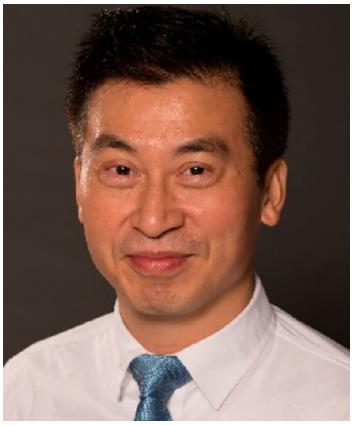

Dr. Yuanbing Mao is a professor of Chemistry at the Illinois Institute of Technology. He received his B.Sc. degree from Xiangtan University, M.Sc. degree from the Institute of Chemistry, Chinese Academy of Sciences, and Ph.D. degree from the State University of

New York at Stony Brook. He has earned several awards, including the Department of Defense Young Investigator Award and the Outstanding Mentorship Award from the Council on Undergraduate Research, and is a recipient of the DOE Visiting Faculty Program. As of today, he has published more than 125 peer-reviewed journal articles as well as some book chapters and patents. His research interests include nanomaterials, solid-state science, and nanoscience with expertise in optoelectronics, energy storage and conversion, and environmental remediation.

■ ACKNOWLEDGMENTS

Y.M. would like to express thanks for the support by the National Science Foundation under CHE (Award Nos. 1952803 and 1710160) and the IIT start-up funds. S.K.G. thanks the United States−India Education Foundation (USIEF, India) and the Institute of International Education (IIE, USA) for his Fulbright Nehru Postdoctoral Fellowship (Award No. 2268/FNPDR/2017).

■ REFERENCES

(1) Darr, J. A.; Zhang, J.; Makwana, N. M.; Weng, X. Continuous Hydrothermal Synthesis of Inorganic Nanoparticles: Applications and Future Directions. *Chem. Rev.* **2017**, *117*, 11125−11238.

(2) Jing, L.; Zhou, W.; Tian, G.; Fu, H. Surface tuning for oxide-based nanomaterials as efficient photocatalysts. *Chem. Soc. Rev.* **2013**, *42*, 9509−9549.

(3) Lee, J.; Yang, J.; Kwon, S. G.; Hyeon, T. Nonclassical nucleation and growth of inorganic nanoparticles. *Nat. Rev. Mater.* **2016**, *1*, 1−16.

(4) Wu, Z.; Yang, S.; Wu, W. Shape control of inorganic nanoparticles from solution. *Nanoscale* **2016**, *8*, 1237−1259.

(5) Gonzalez-Ortiz, D.; Salameh, C.; Bechelany, M.; Miele, P. Nanostructured boron nitride−based materials: synthesis and applications. *Materials Today Advances* **2020**, *8*, 100107.

(6) Cummins, C.; Lundy, R.; Walsh, J. J.; Ponsinet, V.; Fleury, G.; Morris, M. A. Enabling future nanomanufacturing through block copolymer self-assembly: A review. *Nano Today* **2020**, *35*, 100936.

(7) Abdou, M.; Gupta, S. K.; Zuniga, J. P.; Mao, Y. On structure and phase transformation of uranium doped $La_2Hf_2O_7$ nanoparticles as an efficient nuclear waste host. *Materials Chemistry Frontiers* **2018**, *2*, 2201−2211.

(8) Chowdhury, A. R.; Abdullah, A. M.; Hussain, I.; Lopez, J.; Cantu, D.; Gupta, S. K.; Mao, Y.; Danti, S.; Uddin, M. J. Lithium doped zinc oxide based flexible piezoelectric-triboelectric hybrid nanogenerator. *Nano Energy* **2019**, *61*, 327−336.

(9) Gupta, S. K.; Abdou, M.; Zuniga, J. P.; Puretzky, A. A.; Mao, Y. Samarium-Activated $La_2Hf_2O_7$ Nanoparticles as Multifunctional Phosphors. *ACS Omega* **2019**, *4*, 17956−17966.

(10) Gupta, S. K.; Mao, Y. Recent advances, challenges, and opportunities of inorganic nanoscintillators. *Frontiers of Optoelectronics* **2020**, *13*, 156.

(11) Gupta, S. K.; Sudarshan, K.; Modak, B.; Yadav, A. K.; Modak, P.; Jha, S. N.; Bhattacharyya, D. Achieving Bright Blue and Red Luminescence in Ca_2SnO_4 through Defect and Doping Manipulation. *J. Phys. Chem. C* **2020**, *124*, 16090.

(12) Gupta, S. K.; Zuniga, J. P.; Abdou, M.; Ghosh, P.; Mao, Y. Optical properties of undoped, Eu^{3+} doped and Li^{+} co-doped $Y_2Hf_2O_7$ nanoparticles and polymer nanocomposite films. *Inorg. Chem. Front.* **2020**, *7*, 505−518.

(13) Gupta, S. K.; Zuniga, J. P.; Abdou, M.; Thomas, M. P.; De Alwis Goonatilleke, M.; Guiton, B. S.; Mao, Y. Lanthanide-doped lanthanum hafnate nanoparticles as multicolor phosphors for warm white lighting and scintillators. *Chem. Eng. J.* **2020**, *379*, 122314.

(14) Hernandez, C.; Gupta, S. K.; Zuniga, J. P.; Vidal, J.; Galvan, R.; Martinez, M.; Guzman, H.; Chavez, L.; Mao, Y.; Lozano, K. Performance evaluation of Ce^{3+} doped flexible PVDF fibers for efficient optical pressure sensors. *Sens. Actuators, A* **2019**, *298*, 111595.

(15) Srivastava, B. B.; Gupta, S. K.; Li, Y.; Mao, Y. Bright persistent green emitting water-dispersible Zn_2GeO_4:Mn nanorods. *Dalton Transactions* **2020**, *49*, 7328−7340.

(16) Srivastava, B. B.; Gupta, S. K.; Mao, Y. Single red emission from upconverting $ZnGa_2O_4$:Yb,Er nanoparticles co-doped by Cr^{3+}. *J. Mater. Chem. C* **2020**, *8*, 6370−6379.

(17) Srivastava, B. B.; Gupta, S. K.; Mao, Y. Remarkable enhancement of photoluminescence and persistent luminescence of NIR emitting $ZnGa_2O_4$:Cr^{3+} nanoparticles. *CrystEngComm* **2020**, *22*, 2491−2501.

(18) Valdez, M.; Gupta, S. K.; Lozano, K.; Mao, Y. ForceSpun polydiacetylene nanofibers as colorimetric sensor for food spoilage detection. *Sens. Actuators, B* **2019**, *297*, 126734.

(19) Zuniga, J. P.; Gupta, S. K.; Pokhrel, M.; Mao, Y. Exploring the optical properties of $La_2Hf_2O_7$:Pr^{3+} nanoparticles under UV and X-ray excitation for potential lighting and scintillating applications. *New J. Chem.* **2018**, *42*, 9381−9392.

(20) Ariga, K.; Jia, X.; Song, J.; Hill, J. P.; Leong, D. T.; Jia, Y.; Li, J. Nanoarchitectonics beyond Self-Assembly: Challenges to Create Bio-Like Hierarchic Organization. *Angew. Chem., Int. Ed.* **2020**, *59*, 15424−15446.

(21) Bergsman, D. S.; Getachew, B. A.; Cooper, C. B.; Grossman, J. C. Preserving nanoscale features in polymers during laser induced graphene formation using sequential infiltration synthesis. *Nat. Commun.* **2020**, *11*, 3636.

(22) Kamali, A.R., Molten Salt-Assisted Preparation of Nanodiamonds at Atmospheric Pressure, *Green Production of Carbon Nanomaterials in Molten Salts and Applications*; Springer: 2020; pp 141−162;

(23) Konnov, S. V.; Dubray, F.; Clatworthy, E. B.; Kouvatas, C.; Gilson, J.-P.; Dath, J.-P.; Minoux, D.; Aquino, C.; Valtchev, V.; Moldovan, S.; Koneti, S.; Nesterenko, N.; Mintova, S. Novel Strategy for the Synthesis of Ultra-Stable Single-Site Mo-ZSM-5 Zeolite Nanocrystals. *Angew. Chem., Int. Ed.* **2020**, *59*, 19553−19560.

(24) Li, Y.; Zhao, A.; Chen, C.; Zhang, C.; Zhang, J.; Jia, G. Controllable synthesis and morphology-dependent photoluminescence properties of well-defined one-dimensional Zn_2GeO_4:Mn^{2+} nanostructures. *Dyes Pigm.* **2018**, *150*, 267−274.

(25) Nayak, A. K.; Lee, S.; Choi, Y. I.; Yoon, H. J.; Sohn, Y.; Pradhan, D. Crystal phase and size-controlled synthesis of tungsten trioxide hydrate nanoplates at room temperature: enhanced Cr(VI) photoreduction and methylene blue adsorption properties. *ACS Sustainable Chem. Eng.* **2017**, *5*, 2741−2750.

(26) Sundaram, D.; Yang, V.; Yetter, R. A. Metal-based nanoenergetic materials: synthesis, properties, and applications. *Prog. Energy Combust. Sci.* **2017**, *61*, 293−365.

(27) Akkerman, Q. A.; Rainò, G.; Kovalenko, M. V.; Manna, L. Genesis, challenges and opportunities for colloidal lead halide perovskite nanocrystals. *Nat. Mater.* **2018**, *17*, 394.

(28) Richard, B.; Lemyre, J.-L.; Ritcey, A. M. Nanoparticle Size Control in Microemulsion Synthesis. *Langmuir* **2017**, *33*, 4748−4757.

(29) Xin, H.; Namgung, B.; Lee, L. P. Nanoplasmonic optical antennas for life sciences and medicine. *Nature Reviews Materials* **2018**, *3*, 228−243.

(30) Yeom, J.; Santos, U. S.; Chekini, M.; Cha, M.; de Moura, A. F.; Kotov, N. A. Chiromagnetic nanoparticles and gels. *Science* **2018**, *359*, 309−314.

(31) Zhang, H. Ultrathin two-dimensional nanomaterials. *ACS Nano* **2015**, *9*, 9451−9469.

(32) Jeevanandam, J.; Barhoum, A.; Chan, Y. S.; Dufresne, A.; Danquah, M. K. Review on nanoparticles and nanostructured materials: history, sources, toxicity and regulations. *Beilstein J. Nanotechnol.* **2018**, *9*, 1050−1074.

(33) Colvin, V. L. The potential environmental impact of engineered nanomaterials. *Nat. Biotechnol.* **2003**, *21*, 1166−1170.

https://dx.doi.org/10.1021/acs.jpcc.0c10981
J. Phys. Chem. C XXXX, XXX, XXX−XXX

(34) Pastoriza-Santos, I.; Kinnear, C.; Pérez-Juste, J.; Mulvaney, P.; Liz-Marzán, L. M. Plasmonic polymer nanocomposites. *Nature Reviews Materials* **2018**, *3*, 375−391.
(35) Srivastava, R. Synthesis and characterization techniques of nanomaterials. *Int. J. Green Nanotechnol.* **2012**, *4*, 17−27.
(36) Yermakov, A. Y.; Gubkin, A. F.; Korolev, A. V.; Molochnikov, L. S.; Uimin, M. A.; Rosenfeld, E. V.; Kurkin, M. I.; Minin, A. S.; Volegov, A. S.; Boukhvalov, D. W.; et al. Formation of Fe−Fe Antiferromagnetic Dimers in Doped TiO_2:Fe Nanoparticles. *J. Phys. Chem. C* **2019**, *123*, 1494−1505.
(37) Chen, X.; Mao, S. S. Titanium dioxide nanomaterials: synthesis, properties, modifications, and applications. *Chem. Rev.* **2007**, *107*, 2891−2959.
(38) Taloni, A.; Vodret, M.; Costantini, G.; Zapperi, S. Size effects on the fracture of microscale and nanoscale materials, Nature Reviews. *Materials* **2018**, *3*, 211−224.
(39) Cordova, D. L. M.; Fender, S. S.; Kam, T. M.; Seyd, J.; Albrecht, M.; Lu, P.; Fischer, R.; Johnson, D. C. Designed synthesis and structure−property relationships of kinetically stable $[(PbSe)_{1+\delta}]m(VSe_2)_1$ (m = 1, 2, 3, 4) heterostructures. *Chem. Mater.* **2019**, *31*, 8473−8483.
(40) Zhang, K.; Feng, Y.; Wang, F.; Yang, Z.; Wang, J. Two dimensional hexagonal boron nitride (2D-hBN): synthesis, properties and applications. *J. Mater. Chem. C* **2017**, *5*, 11992−12022.
(41) Li, H.; Zhou, X.; Zhai, W.; Lu, S.; Liang, J.; He, Z.; Long, H.; Xiong, T.; Sun, H.; He, Q.; et al. Phase Engineering of Nanomaterials for Clean Energy and Catalytic Applications. *Adv. Energy Mater.* **2020**, *10*, 2002019.
(42) Chen, Y.; Lai, Z.; Zhang, X.; Fan, Z.; He, Q.; Tan, C.; Zhang, H. Phase engineering of nanomaterials. *Nature Reviews Chemistry* **2020**, *4*, 243−256.
(43) Amorim, C. A.; Gozzi, G.; Chinaglia, D. L.; dos Santos, F. J.; Santos, L. F. Synthesis of Transparent Semiconducting Metal-oxides via Polymeric Precursor Route for Application in Thin-film Field-Effect Transistors. *MRS Advances* **2016**, *1*, 489−494.
(44) Zuniga, J. P.; Abdou, M.; Gupta, S. K.; Mao, Y. Molten-Salt Synthesis of Complex Metal Oxide Nanoparticles. *J. Visualized Exp.* **2018**, e58482.
(45) Feinle, A.; Elsaesser, M. S.; Hüsing, N. Sol−gel synthesis of monolithic materials with hierarchical porosity. *Chem. Soc. Rev.* **2016**, *45*, 3377−3399.
(46) Hachani, R.; Lowdell, M.; Birchall, M.; Hervault, A.; Mertz, D.; Begin-Colin, S.; Thanh, N. T. K. Polyol synthesis, functionalisation, and biocompatibility studies of superparamagnetic iron oxide nanoparticles as potential MRI contrast agents. *Nanoscale* **2016**, *8*, 3278−3287.
(47) Kirubasankar, B.; Vijayan, S.; Angaiah, S. Sonochemical synthesis of a 2D−2D $MoSe_2$/graphene nanohybrid electrode material for asymmetric supercapacitors. *Sustainable Energy & Fuels* **2019**, *3*, 467−477.
(48) Theiss, F. L.; Ayoko, G. A.; Frost, R. L. Synthesis of layered double hydroxides containing Mg^{2+}, Zn^{2+}, Ca^{2+} and Al^{3+} layer cations by co-precipitation methods—A review. *Appl. Surf. Sci.* **2016**, *383*, 200−213.
(49) Varma, A.; Mukasyan, A. S.; Rogachev, A. S.; Manukyan, K. V. Solution Combustion Synthesis of Nanoscale Materials. *Chem. Rev.* **2016**, *116*, 14493−14586.
(50) Chamorro, J. R.; McQueen, T. M. Progress toward Solid State Synthesis by Design. *Acc. Chem. Res.* **2018**, *51*, 2918−2925.
(51) Gupta, S. K.; Kadam, R.; Pujari, P. Lanthanide spectroscopy in probing structure-property correlation in multi-site photoluminescent phosphors. *Coord. Chem. Rev.* **2020**, *420*, 213405.
(52) Gupta, S. K.; Mao, Y. Molten salt synthesis of metal oxide nanomaterials: status, opportunity, and challenge. *Prog. Mater. Sci.* **2020**, 100734.
(53) Beyene, A. M.; Baek, C.; Jung, W. K.; Ragupathy, P.; Kim, D. K. Understanding the role of oxygen ion (O^{2-}) activity in 1-D crystal growth of rutile TiO_2 in molten salts. *CrystEngComm* **2018**, *20*, 487−495.
(54) Boltersdorf, J.; King, N.; Maggard, P. A. Flux-mediated crystal growth of metal oxides: synthetic tunability of particle morphologies, sizes, and surface features for photocatalysis research. *CrystEngComm* **2015**, *17*, 2225−2241.
(55) Ahn, E. C.; Wong, H.-S. P.; Pop, E. Carbon nanomaterials for non-volatile memories. *Nat. Rev. Mater.* **2018**, *3*, 1−15.
(56) Cai, Y.; Wei, Z.; Song, C.; Tang, C.; Han, W.; Dong, X. Optical nano-agents in the second near-infrared window for biomedical applications. *Chem. Soc. Rev.* **2019**, *48*, 22−37.
(57) Dey, G.; Yang, L.; Lee, K.-B.; Wang, L. Characterizing molecular adsorption on biodegradable MnO_2 nanoscaffolds. *J. Phys. Chem. C* **2018**, *122*, 29017−29027.
(58) Ghodsi, V.; Lu, W.; Radovanovic, P. V. Synergistic Effect of the Electronic Structure and Defect Formation Enhances Photocatalytic Efficiency of Gallium Tin Oxide Nanocrystals. *J. Phys. Chem. C* **2019**, *123*, 433−442.
(59) Gogotsi, Y. *Nanomaterials handbook*; CRC press: 2006.
(60) Mao, Y.; Park, T. J.; Zhang, F.; Zhou, H.; Wong, S. S. Environmentally friendly methodologies of nanostructure synthesis. *Small* **2007**, *3*, 1122−1139.
(61) Mao, Y.; Park, T.-J.; Wong, S. S. Synthesis of classes of ternary metal oxide nanostructures. *Chem. Commun.* **2005**, 5721−5735.
(62) Li, L.; Deng, J.; Chen, J.; Xing, X. Topochemical molten salt synthesis for functional perovskite compounds. *Chemical science* **2016**, *7*, 855−865.
(63) Afanasiev, P.; Geantet, C. Synthesis of solid materials in molten nitrates. *Coord. Chem. Rev.* **1998**, *178*, 1725−1752.
(64) Bugaris, D. E.; zur Loye, H. C. Materials discovery by flux crystal growth: quaternary and higher order oxides. *Angew. Chem., Int. Ed.* **2012**, *51*, 3780−3811.
(65) Gonzalo-Juan, I.; Riedel, R. Ceramic synthesis from condensed phases. *ChemTexts* **2016**, *2*, 6.
(66) Liu, X.; Fechler, N.; Antonietti, M. Salt melt synthesis of ceramics, semiconductors and carbon nanostructures. *Chem. Soc. Rev.* **2013**, *42*, 8237−8265.
(67) Xue, P.; Wu, H.; Lu, Y.; Zhu, X. Recent progress in molten salt synthesis of low-dimensional perovskite oxide nanostructures, structural characterization, properties, and functional applications: a review. *J. Mater. Sci. Technol.* **2018**, *34*, 914−930.
(68) Chen, D. P.; Fu, J.; Skrabalak, S. E. Towards Shape Control of Metal Oxide Nanocrystals in Confined Molten Media. *ChemNanoMat* **2015**, *1*, 18−26.
(69) Azov, V. A.; Egorova, K. S.; Seitkalieva, M. M.; Kashin, A. S.; Ananikov, V. P. Solvent-in-salt" systems for design of new materials in chemistry, biology and energy research. *Chem. Soc. Rev.* **2018**, *47*, 1250−1284.
(70) Einarsrud, M.-A.; Grande, T. 1D oxide nanostructures from chemical solutions. *Chem. Soc. Rev.* **2014**, *43*, 2187−2199.
(71) Patzke, G. R.; Zhou, Y.; Kontic, R.; Conrad, F. Oxide nanomaterials: synthetic developments, mechanistic studies, and technological innovations. *Angew. Chem., Int. Ed.* **2011**, *50*, 826−859.
(72) Fu, J.; DeSantis, C. J.; Weiner, R. G.; Skrabalak, S. E. Aerosol-Assisted Synthesis of Shape-Controlled $CoFe_2O_4$: Topotactic versus Direct Melt Crystallization. *Chem. Mater.* **2015**, *27*, 1863−1868.
(73) Fu, J.; Skrabalak, S. E. Aerosol synthesis of shape-controlled template particles: a route to Ta_3N_5 nanoplates and octahedra as photocatalysts. *J. Mater. Chem. A* **2016**, *4*, 8451−8457.
(74) Mann, A. K. P.; Fu, J.; DeSantis, C. J.; Skrabalak, S. E. Spatial and Temporal Confinement of Salt Fluxes for the Shape-Controlled Synthesis of Fe_2O_3 Nanocrystals. *Chem. Mater.* **2013**, *25*, 1549−1555.
(75) Mann, A. K. P.; Wicker, S.; Skrabalak, S. E. Aerosol-Assisted Molten Salt Synthesis of $NaInS_2$ Nanoplates for Use as a New Photoanode Material. *Adv. Mater.* **2012**, *24*, 6186−6191.
(76) Ceravola, R.; Oró-Solé, J.; Black, A. P.; Ritter, C.; Puente Orench, I.; Mata, I.; Molins, E.; Frontera, C.; Fuertes, A.

https://dx.doi.org/10.1021/acs.jpcc.0c10981
J. Phys. Chem. C XXXX, XXX, XXX−XXX

Topochemical synthesis of cation ordered double perovskite oxynitrides. *Dalton Transactions* **2017**, *46*, 5128−5132.
(77) Fu, J.; Hou, Y.; Zheng, M.; Zhu, M. Topochemical build-up of $BaTiO_3$ nanorods using $BaTi_2O_5$ as the template. *CrystEngComm* **2017**, *19*, 1115−1122.
(78) Fu, J.; Hou, Y.; Zheng, M.; Zhu, M. Regulation of the Ba/Sr Ratio of (Ba,Sr)TiO_3 and Nanorod Build-Up through a Topochemical Synthesis Method Using $BaTi_2O_5$ as the Template. *Eur. J. Inorg. Chem.* **2018**, *2018*, 3088−3094.
(79) Lee, K. T.; Ramesh, T. N.; Nan, F.; Botton, G.; Nazar, L. F. Topochemical Synthesis of Sodium Metal Phosphate Olivines for Sodium-Ion Batteries. *Chem. Mater.* **2011**, *23*, 3593−3600.
(80) He, S.; Du, H.; Wang, K.; Liu, Q.; Sun, J.; Liu, Y.; Du, Z.; Xie, L.; Ai, W.; Huang, W. Low-temperature molten salt synthesis of MoS_2@CoS_2 heterostructures for efficient hydrogen evolution reaction. *Chem. Commun.* **2020**, *56*, 5548−5551.
(81) Kamysbayev, V.; Srivastava, V.; Ludwig, N. B.; Borkiewicz, O. J.; Zhang, H.; Ilavsky, J.; Lee, B.; Chapman, K. W.; Vaikuntanathan, S.; Talapin, D. V. Nanocrystals in Molten Salts and Ionic Liquids: Experimental Observation of Ionic Correlations Extending beyond the Debye Length. *ACS Nano* **2019**, *13*, 5760−5770.
(82) Kimura, T. Molten salt synthesis of ceramic powders. *Advances in Ceramics-Synthesis and Characterization, Processing and Specific Applications* **2011**, 75−100.
(83) Qiu, W.; Liu, Y.; Ye, J.; Fan, H.; Wang, G. Molten salt synthesis and growth mechanism of WC platelet powders. *Powder Technol.* **2017**, *310*, 228−233.
(84) Roy, B.; Ahrenkiel, S. P.; Fuierer, P. A. Controlling the size and morphology of TiO_2 powder by molten and solid salt synthesis. *J. Am. Ceram. Soc.* **2008**, *91*, 2455−2463.
(85) Fu, J.; Hou, Y.; Liu, X.; Zheng, M.; Zhu, M. A construction strategy of ferroelectrics by the molten salt method and its application in the energy field. *J. Mater. Chem. C* **2020**, *8*, 8704−8731.
(86) Sanjaya Ranmohotti, K.; Josepha, E.; Choi, J.; Zhang, J.; Wiley, J. B. Topochemical Manipulation of Perovskites: Low-Temperature Reaction Strategies for Directing Structure and Properties. *Adv. Mater.* **2011**, *23*, 442−460.
(87) Xiao, X.; Wang, H.; Urbankowski, P.; Gogotsi, Y. Topochemical synthesis of 2D materials. *Chem. Soc. Rev.* **2018**, *47*, 8744−8765.
(88) Rørvik, P. M.; Grande, T.; Einarsrud, M. A. One-dimensional nanostructures of ferroelectric perovskites. *Adv. Mater.* **2011**, *23*, 4007−4034.
(89) Elwell, D.; Schell, H. *Crystal Growth from High Temperature Solutions*; Acad. Press: London, 1975.
(90) Elwell, D.; Neate, B. Mechanisms of crystal growth from fluxed melts. *J. Mater. Sci.* **1971**, *6*, 1499−1519.
(91) Corbett, J. D. Fused Salt Chemistry. *Surv. Prog. Chem.* **1964**, *2*, 91−154.
(92) Choi, J.; King, N.; Maggard, P. A. Metastable Cu(I)-niobate semiconductor with a low-temperature, nanoparticle-mediated synthesis. *ACS Nano* **2013**, *7*, 1699−1708.
(93) Fuoco, L.; Joshi, U. A.; Maggard, P. A. Preparation and photoelectrochemical properties of p-type $Cu_5Ta_{11}O_{30}$ and $Cu_3Ta_7O_{19}$ semiconducting polycrystalline films. *J. Phys. Chem. C* **2012**, *116*, 10490−10497.
(94) Joshi, U. A.; Maggard, P. A. $CuNb_3O_8$: a p-type semiconducting metal oxide photoelectrode. *J. Phys. Chem. Lett.* **2012**, *3*, 1577−1581.
(95) Joshi, U. A.; Palasyuk, A. M.; Maggard, P. A. Photoelectrochemical Investigation and Electronic Structure of a p-Type $CuNbO_3$ Photocathode, The. *J. Phys. Chem. C* **2011**, *115*, 13534−13539.
(96) King, N.; Sahoo, P. P.; Fuoco, L.; Stuart, S.; Dougherty, D.; Liu, Y.; Maggard, P. A. Copper Deficiency in the p-Type Semiconductor $Cu_{1-x}Nb_3O_8$. *Chem. Mater.* **2014**, *26*, 2095−2104.
(97) McLamb, N.; Sahoo, P. P.; Fuoco, L.; Maggard, P. A. Flux growth of single-crystal $Na_2Ta_4O_{11}$ particles and their photocatalytic hydrogen production. *Cryst. Growth Des.* **2013**, *13*, 2322−2326.
(98) Palasyuk, O.; Palasyuk, A.; Maggard, P. A. Syntheses, optical properties and electronic structures of copper(I) tantalates: $Cu_5Ta_{11}O_{30}$ and $Cu_3Ta_7O_{19}$. *J. Solid State Chem.* **2010**, *183*, 814−822.
(99) Palasyuk, O.; Palasyuk, A.; Maggard, P. A. Site-Differentiated Solid Solution in $(Na_{1-x}Cu_x)_2Ta_4O_{11}$ and Its Electronic Structure and Optical Properties. *Inorg. Chem.* **2010**, *49*, 10571−10578.
(100) Porob, D. G.; Maggard, P. A. Flux syntheses of La-doped $NaTaO_3$ and its photocatalytic activity. *J. Solid State Chem.* **2006**, *179*, 1727−1732.
(101) Sahoo, P. P.; Maggard, P. A. Crystal chemistry, band engineering, and photocatalytic activity of the $LiNb_3O_8$−$CuNb_3O_8$ solid solution. *Inorg. Chem.* **2013**, *52*, 4443−4450.
(102) Penilla Garcia, M. A.; Gupta, S. K.; Mao, Y. Effects of molten-salt processing parameters on the structural and optical properties of preformed $La_2Zr_2O_7$:Eu^{3+} nanoparticles. *Ceram. Int.* **2020**, *46*, 1352−1361.
(103) Reddy, M. V.; Rajesh, M.; Adams, S.; Chowdari, B. V. R. Effect of Initial Reactants and Reaction Temperature on Molten Salt Synthesis of $CuCo_2O_4$ and Its Sustainable Energy Storage Properties. *ACS Sustainable Chem. Eng.* **2016**, *4*, 3076−3086.
(104) Bale, C.; Bélisle, E.; Chartrand, P.; Decterov, S.; Eriksson, G.; Hack, K.; Jung, I.-H.; Kang, Y.-B.; Melançon, J.; Pelton, A.; et al. FactSage thermochemical software and databases—recent developments. *CALPHAD: Comput. Coupling Phase Diagrams Thermochem.* **2009**, *33*, 295−311.
(105) Flood, H.; Förland, T.; et al. The acidic and basic properties of oxides. *Acta Chem. Scand.* **1947**, *1*, 592−604.
(106) Mugavero, S. J., III; Gemmill, W. R.; Roof, I. P.; zur Loye, H.-C. Materials discovery by crystal growth: Lanthanide metal containing oxides of the platinum group metals (Ru, Os, Ir, Rh, Pd, Pt) from molten alkali metal hydroxides. *J. Solid State Chem.* **2009**, *182*, 1950−1963.
(107) Canfield, P.C., Solution growth of intermetallic single crystals: A beginner's guide, *Properties and Applications of Complex Intermetallics*; World Scientific, 2009; pp 293−111.
(108) Chance, W. M.; Bugaris, D. E.; Sefat, A. S.; zur Loye, H.-C. Crystal growth of new hexahydroxometallates using a hydroflux. *Inorg. Chem.* **2013**, *52*, 11723−11733.
(109) Kanatzidis, M. G. Molten alkali-metal polychalcogenides as reagents and solvents for the synthesis of new chalcogenide materials. *Chem. Mater.* **1990**, *2*, 353−363.
(110) Kanatzidis, M. G. New directions in synthetic solid state chemistry: chalcophosphate salt fluxes for discovery of new multinary solids. *Curr. Opin. Solid State Mater. Sci.* **1997**, *2*, 139−149.
(111) McCarthy, T. J.; Kanatzidis, M. G. Use of molten alkali-metal polythiophosphate fluxes for synthesis at intermediate temperatures. Isolation and structural characterization of $ABiP_2S_7$ (A = K, Rb). *Chem. Mater.* **1993**, *5*, 1061−1063.
(112) McCarthy, T. J.; Ngeyi, S. P.; Liao, J. H.; DeGroot, D. C.; Hogan, T.; Kannewurf, C. R.; Kanatzidis, M. G. Molten salt synthesis and properties of three new solid-state ternary bismuth chalcogenides,. beta.-$CsBiS_2$, gamma.-$CsBiS_2$, and $K_2Bi_8Se_{13}$. *Chem. Mater.* **1993**, *5*, 331−340.
(113) Phelan, W. A.; Menard, M. C.; Kangas, M. J.; McCandless, G. T.; Drake, B. L.; Chan, J. Y. Adventures in crystal growth: synthesis and characterization of single crystals of complex intermetallic compounds. *Chem. Mater.* **2012**, *24*, 409−420.
(114) Schmitt, D. C.; Kangas, M. J.; Chan, J. Y. *Discovery and Single Crystal Growth of Lanthanide Intermetallics—Interplay of Synthesis and Physical Properties*; https://www.sigmaaldrich.com/technical-documents/articles/materials-science/discovery-and-single-crystal-growth.html.
(115) Willert, M.; Rothe, R.; Landfester, K.; Antonietti, M. Synthesis of inorganic and metallic nanoparticles by miniemulsifi-

cation of molten salts and metals. *Chem. Mater.* **2001**, *13*, 4681−4685.
(116) Lux, H. "Acids" and "bases" in a fused salt bath: the determination of oxygen-ion concentration. *Z. Elektrochem. Soc.* **1939**, *45*, 303−310.
(117) Banerjee, S.; Malliakas, C. D.; Kanatzidis, M. G. New layered tin (II) thiophosphates $ASnPS_4$ (A = K, Rb, Cs): Synthesis, structure, glass formation, and the modulated $CsSnPS_4$. *Inorg. Chem.* **2012**, *51*, 11562−11573.
(118) Shoemaker, D. P.; Chung, D. Y.; Mitchell, J.; Bray, T. H.; Soderholm, L.; Chupas, P. J.; Kanatzidis, M. G. Understanding fluxes as media for directed synthesis: In situ local structure of molten potassium polysulfides. *J. Am. Chem. Soc.* **2012**, *134*, 9456−9463.
(119) Sunshine, S. A.; Kang, D.; Ibers, J. A. A new low-temperature route to metal polychalcogenides: solid-state synthesis of $K_4Ti_3S_{14}$, a novel one-dimensional compound. *J. Am. Chem. Soc.* **1987**, *109*, 6202−6204.
(120) Urben, P. *Bretherick's handbook of reactive chemical hazards*; Elsevier: 2017.
(121) Helan, M.; Berchmans, L. J.; Jose, T. P.; Visuvasam, A.; Angappan, S. Molten salt synthesis of $LiMn_2O_4$ using chloride−carbonate melt. *Mater. Chem. Phys.* **2010**, *124*, 439−442.
(122) Schaak, R. E.; Mallouk, T. E. Topochemical synthesis of three-dimensional perovskites from lamellar precursors. *J. Am. Chem. Soc.* **2000**, *122*, 2798−2803.
(123) Boltersdorf, J.; Wong, T.; Maggard, P. A. Synthesis and optical properties of Ag(I), Pb(II), and Bi(III) tantalate-based photocatalysts. *ACS Catal.* **2013**, *3*, 2943−2953.
(124) Geselbracht, M. J.; Walton, R. I.; Cowell, E. S.; Millange, F.; O'Hare, D. An investigation of the synthesis of the layered perovskite $RbCa_2Nb_3O_{10}$ using time-resolved in situ high-temperature powder X-ray diffraction. *Chem. Mater.* **2002**, *14*, 4343−4349.
(125) Geselbracht, M. J.; Noailles, L. D.; Ngo, L. T.; Pikul, J. H.; Walton, R. I.; Cowell, E. S.; Millange, F.; O'Hare, D. Probing molten salt flux reactions using time-resolved in situ high-temperature powder X-ray diffraction: A new synthesis route to the mixed-valence $NaTi_2O_4$. *Chem. Mater.* **2004**, *16*, 1153−1159.
(126) Yoon, K. H.; Cho, Y. S.; Kang, D. H. Molten salt synthesis of lead-based relaxors. *J. Mater. Sci.* **1998**, *33*, 2977−2984.
(127) Kimura, T.; Yamaguchi, T. Morphology of Bi_2WO_6 powders obtained in the presence of fused salts. *J. Mater. Sci.* **1982**, *17*, 1863−1870.
(128) Akdogan, E.; Brennan, R. E.; Allahverdi, M.; Safari, A. Effects of molten salt synthesis (MSS) parameters on the morphology of $Sr_3Ti_2O_7$ and $SrTiO_3$ seed crystals. *J. Electroceram.* **2006**, *16*, 159−165.
(129) Hayashi, Y.; Kimura, T.; Yamaguchi, T. Preparation of rod-shaped $BaTiO_3$ powder. *J. Mater. Sci.* **1986**, *21*, 757−762.
(130) Kimura, T.; Takahashi, T.; Yamaguchi, T. Preparation and characteristics of Ni-ferrite powders obtained in the presence of fused salts. *J. Mater. Sci.* **1980**, *15*, 1491−1497.
(131) Onoda, G.Y., Jr.; Hench, L.L. *The Science of Ceramic Processing Before Firing*; Department of Materials Science and Engineering, University of Florida: Gainesville, FL, 1977.
(132) Cherginets, V. Studies of cation−oxide ion interactions in halide melts. The potentiometric control of saturation at different oxide ion concentrations. *J. Electroanal. Chem.* **2000**, *493*, 144−147.
(133) Cherginets, V.; Khailova, E. On the solubilities of bivalent metal oxides in molten alkaline chlorides. *Electrochim. Acta* **1994**, *39*, 823−829.
(134) Cherginets, V.; Rebrova, T.; Naumenko, V. On metal oxide solubilities in some molten alkali metal bromides at T = 973 K, The. *J. Chem. Thermodyn.* **2014**, *74*, 216−220.
(135) Ishitsuka, T.; Nose, K. Stability of protective oxide films in waste incineration environment—solubility measurement of oxides in molten chlorides. *Corros. Sci.* **2002**, *44*, 247−263.
(136) Masset, P.; Guidotti, R. A. Thermal activated (thermal) battery technology: Part II. Molten salt electrolytes. *J. Power Sources* **2007**, *164*, 397−414.
(137) Nakamura, S.; Iwasawa, K.; Morita, K.; Sano, N. The influence of basicity on the solubility of platinum in oxide melts. *Metall. Mater. Trans. B* **1998**, *29*, 411−414.
(138) Orfield, M.; Shores, D. A. The solubility of NiO in binary mixtures of molten carbonates. *J. Electrochem. Soc.* **1989**, *136*, 2862.
(139) Qingfeng, L.; Borup, F.; Petrushina, I.; Bjerrum, N. J. Complex formation during dissolution of metal oxides in molten alkali carbonates. *J. Electrochem. Soc.* **1999**, *146*, 2449.
(140) Skryptun, I. N. CuO Solubility in Alkali-Chloride Melts. *ECS Trans.* **2010**, *33*, 303.
(141) Zinchenko, V.; Timukhin, E.; Pavlinchuk, S.; Nechiporenko, A.; Sadkovskaya, L. Basicity-acidity and solubility of metal fluorides and oxides in salt melts. *Russ. J. Electrochem.* **2012**, *48*, 995−999.
(142) Sundermeyer, W. Fused salts and their use as reaction media. *Angew. Chem., Int. Ed. Engl.* **1965**, *4*, 222−238.
(143) Ahmed, J.; Mao, Y. Ultrafine iridium oxide nanorods synthesized by molten salt method toward electrocatalytic oxygen and hydrogen evolution reactions. *Electrochim. Acta* **2016**, *212*, 686−693.
(144) Mao, Y. Facile molten-salt synthesis of double perovskite La_2BMO_6 nanoparticles. *RSC Adv.* **2012**, *2*, 12675−12678.
(145) Mao, Y.; Parsons, J.; McCloy, J. S. Magnetic properties of double perovskite La_2BMnO_6 (B = Ni or Co) nanoparticles. *Nanoscale* **2013**, *5*, 4720−4728.
(146) Santra, S.; Das, N. S.; Das, B.; Banerjee, D.; Chattopadhyay, K. K. Synthesis of $CuBO_2$ nano/microrods via easy molten salt route and study of its field emission properties. *Cryst. Growth Des.* **2015**, *15*, 1518−1525.
(147) Lu, X.; Lin, X.; Shang, Y.; Huang, T.; Yu, A. Modified KCl molten salt method synthesis of spinel $LiNi_{0.5}Mn_{1.5}O_4$ with loose structure as cathodes for Li-ion batteries. *Int. J. Electrochem. Sci.* **2014**, *9*, 7253−7265.
(148) Corr, S. A. Metal oxide nanoparticles. *Nanoscience* **2013**, *2*, 204−224.
(149) Fernández-García, M.; Rodriguez, J. A. Metal oxide nanoparticles. *Encyclopedia of inorganic and bioinorganic chemistry* **2011**, DOI: 10.1002/9781119951438.eibc0331.
(150) Hendraningrat, L.; Torsæter, O. Metal oxide-based nanoparticles: revealing their potential to enhance oil recovery in different wettability systems. *Appl. Nanosci.* **2015**, *5*, 181−199.
(151) Khalil, M.; Jan, B. M.; Tong, C. W.; Berawi, M. A. Advanced nanomaterials in oil and gas industry: design, application and challenges. *Appl. Energy* **2017**, *191*, 287−310.
(152) Metin, C. O.; Baran, J. R.; Nguyen, Q. P. Adsorption of surface functionalized silica nanoparticles onto mineral surfaces and decane/water interface. *J. Nanopart. Res.* **2012**, *14*, 1246.
(153) Nguyen, N. H.; Padil, V. V. T.; Slaveykova, V. I.; Černík, M.; Ševců, A. Green synthesis of metal and metal oxide nanoparticles and their effect on the unicellular alga Chlamydomonas reinhardtii. *Nanoscale Res. Lett.* **2018**, *13*, 1−13.
(154) Xue, Z.; Foster, E.; Wang, Y.; Nayak, S.; Cheng, V.; Ngo, V. W.; Pennell, K. D.; Bielawski, C. W.; Johnston, K. P. Effect of grafted copolymer composition on iron oxide nanoparticle stability and transport in porous media at high salinity. *Energy Fuels* **2014**, *28*, 3655−3665.
(155) Xu, J.; Zhu, G.; Lin, T.; Hong, Z.; Wang, J.; Huang, F. Molten salt assisted synthesis of black titania hexagonal nanosheets with tuneable phase composition and morphology. *RSC Adv.* **2015**, *5*, 85928−85932.
(156) Li, T.; Xu, Y.; Qian, X.; Yue, Q.; Kang, Y. Low-Temperature Molten Salt Synthesis for Ligand-Free Transition Metal Oxide Nanoparticles, ACS Applied Energy. *Materials* **2020**, *3*, 3984−3990.
(157) Reddy, N. L.; Emin, S.; Kumari, V. D.; Muthukonda Venkatakrishnan, S. Venkatakrishnan, CuO quantum dots decorated TiO_2 nanocomposite photocatalyst for stable hydrogen generation. *Ind. Eng. Chem. Res.* **2018**, *57*, 568−577.

(158) Hu, Z.; Xiao, X.; Jin, H.; Li, T.; Chen, M.; Liang, Z.; Guo, Z.; Li, J.; Wan, J.; Huang, L.; et al. Rapid mass production of two-dimensional metal oxides and hydroxides via the molten salts method. *Nat. Commun.* **2017**, *8*, 15630.
(159) Mao, Y.; Yang, X.; Gong, W.; Zhang, J.; Pan, T.; Sun, H.; Chen, Z.; Wang, Z.; Zhu, J.; Hu, J.; et al. A Dopant Replacement-Driven Molten Salt Method toward the Synthesis of Sub-5-nm-Sized Ultrathin Nanowires. *Small* **2020**, *16*, 2001098.
(160) Gupta, S. K.; Zuniga, J. P.; Abdou, M.; Mao, Y. Thermal annealing effects on $La_2Hf_2O_7$:Eu^{3+} nanoparticles: a curious case study of structural evolution and site-specific photo-and radio-luminescence. *Inorg. Chem. Front.* **2018**, *5*, 2508−2521.
(161) Gupta, S. K.; Zuniga, J. P.; Ghosh, P. S.; Abdou, M.; Mao, Y. Correlating Structure and Luminescence Properties of Undoped and Eu^{3+}-Doped $La_2Hf_2O_7$ Nanoparticles Prepared with Different Coprecipitating pH Values through Experimental and Theoretical Studies. *Inorg. Chem.* **2018**, *57*, 11815−11830.
(162) Zuniga, J. P.; Gupta, S. K.; Abdou, M.; Mao, Y. Effect of molten salt synthesis processing duration on the photo-and radioluminescence of UV-, visible-, and X-ray-excitable $La_2Hf_2O_7$:Eu^{3+} nanoparticles. *ACS Omega* **2018**, *3*, 7757−7770.
(163) Banerjee, S.; Kim, D.-I.; Robinson, R. D.; Herman, I. P.; Mao, Y.; Wong, S. S. Observation of Fano asymmetry in Raman spectra of $SrTiO_3$ and $Ca_xSr_{1-x}TiO_3$ perovskite nanocubes. *Appl. Phys. Lett.* **2006**, *89*, 223130.
(164) Berweger, S.; Neacsu, C. C.; Mao, Y.; Zhou, H.; Wong, S. S.; Raschke, M. B. Optical nanocrystallography with tip-enhanced phonon Raman spectroscopy. *Nat. Nanotechnol.* **2009**, *4*, 496−499.
(165) Gupta, S. K.; Grover, V.; Shukla, R.; Srinivasu, K.; Natarajan, V.; Tyagi, A. Exploring pure and RE co-doped (Eu^{3+}, Tb^{3+} and Dy^{3+}) gadolinium scandate: Luminescence behaviour and dynamics of energy transfer. *Chem. Eng. J.* **2016**, *283*, 114−126.
(166) Gupta, S. K.; Kadam, R.; Natarajan, V.; Godbole, S. Nanoparticles of $Sr_{0.995}Gd_{0.005}ZrO_3$-gel-combustion synthesis, characterization, fluorescence and EPR spectroscopy. *Mater. Sci. Eng., B* **2014**, *183*, 6−11.
(167) Gupta, S. K.; Pathak, N.; Gupta, R.; Thulasidas, S.; Natarajan, V. Probing the oxidation state and coordination geometry of uranium ion in $SrZrO_3$ perovskite. *J. Mol. Struct.* **2014**, *1068*, 204−209.
(168) Mao, Y.; Banerjee, S.; Wong, S. S. Large-scale synthesis of single-crystalline perovskite nanostructures. *J. Am. Chem. Soc.* **2003**, *125*, 15718−15719.
(169) Mao, Y.; Banerjee, S.; Wong, S. S. Hydrothermal synthesis of perovskite nanotubes. *Chem. Commun.* **2003**, 408−409.
(170) Mao, Y.; Wong, S. S. Composition and shape control of crystalline $Ca_{1-x}Sr_xTiO_3$ perovskite nanoparticles. *Adv. Mater.* **2005**, *17*, 2194−2199.
(171) Park, T.-J.; Mao, Y.; Wong, S. S. Synthesis and characterization of multiferroic $BiFeO_3$ nanotubes. *Chem. Commun.* **2004**, 2708−2709.
(172) Zhou, H.; Mao, Y.; Wong, S. S. Probing structure−parameter correlations in the molten salt synthesis of $BaZrO_3$ perovskite submicrometer-sized particles. *Chem. Mater.* **2007**, *19*, 5238−5249.
(173) Zhou, H.; Mao, Y.; Wong, S. S. Shape control and spectroscopy of crystalline $BaZrO_3$ perovskite particles. *J. Mater. Chem.* **2007**, *17*, 1707−1713.
(174) Xue, P.; Wu, H.; Lu, Y.; Zhu, X. Recent progress in molten salt synthesis of low-dimensional perovskite oxide nanostructures, structural characterization, properties, and functional applications: A review. *J. Mater. Sci. Technol.* **2018**, *34*, 914−930.
(175) Cheng, L.-Q.; Li, J.-F. A review on one dimensional perovskite nanocrystals for piezoelectric applications. *Journal of Materiomics* **2016**, *2*, 25−36.
(176) Wu, H.; Xia, W.; Xue, P.; Zhu, X. Perovskite oxide nanocrystals: Synthesis, characterization, physical properties, and applications. *Ferroelectrics* **2017**, *518*, 127−136.
(177) Gonell, F.; Alem, N.; Dunne, P.; Crochet, G.; Beaunier, P.; Méthivier, C.; Montero, D.; Laberty-Robert, C.; Doudin, B.; Portehault, D. Versatile Molten Salt Synthesis of Manganite Perovskite Oxide Nanocrystals and Their Magnetic Properties. *ChemNanoMat* **2019**, *5*, 358−363.
(178) Jiang, B.; Iocozzia, J.; Zhao, L.; Zhang, H.; Harn, Y.-W.; Chen, Y.; Lin, Z. Barium titanate at the nanoscale: controlled synthesis and dielectric and ferroelectric properties. *Chem. Soc. Rev.* **2019**, *48*, 1194−1228.
(179) Song, W.; Salvador, P. A.; Rohrer, G. S. Influence of the Magnitude of Ferroelectric Domain Polarization on the Photochemical Reactivity of $BaTiO_3$. *ACS Appl. Mater. Interfaces* **2018**, *10*, 41450−41457.
(180) Li, T.; Lipatov, A.; Lu, H.; Lee, H.; Lee, J.-W.; Torun, E.; Wirtz, L.; Eom, C.-B.; Íñiguez, J.; Sinitskii, A.; et al. Optical control of polarization in ferroelectric heterostructures. *Nat. Commun.* **2018**, *9*, 3344.
(181) Defay, E.; Faye, R.; Despesse, G.; Strozyk, H.; Sette, D.; Crossley, S.; Moya, X.; Mathur, N. D. Enhanced electrocaloric efficiency via energy recovery, Nature. *Nat. Commun.* **2018**, *9*, 1827.
(182) Wang, L.; Feng, Q.; Kim, Y.; Kim, R.; Lee, K. H.; Pollard, S. D.; Shin, Y. J.; Zhou, H.; Peng, W.; Lee, D.; Meng, W.; Yang, H.; Han, J. H.; Kim, M.; Lu, Q.; Noh, T. W. Ferroelectrically tunable magnetic skyrmions in ultrathin oxide heterostructures. *Nat. Mater.* **2018**, *17*, 1087−1094.
(183) Jang, S.; Oh, J. H. Rapid Fabrication of Microporous $BaTiO_3$/PDMS Nanocomposites for Triboelectric Nanogenerators through One-step Microwave Irradiation. *Sci. Rep.* **2018**, *8*, 14287.
(184) Malakooti, M. H.; Julé, F.; Sodano, H. A. Printed Nanocomposite Energy Harvesters with Controlled Alignment of Barium Titanate Nanowires. *ACS Appl. Mater. Interfaces* **2018**, *10*, 38359−38367.
(185) Wu, J.; Qin, N.; Yuan, B.; Lin, E.; Bao, D. Enhanced Pyroelectric Catalysis of $BaTiO_3$ Nanowires for Utilizing Waste Heat in Pollution Treatment. *ACS Appl. Mater. Interfaces* **2018**, *10*, 37963−37973.
(186) Wu, J.; Qin, N.; Bao, D. Effective enhancement of piezocatalytic activity of $BaTiO_3$ nanowires under ultrasonic vibration. *Nano Energy* **2018**, *45*, 44−51.
(187) Demircivi, P.; Simsek, E. B. Visible-light-enhanced photoactivity of perovskite-type W-doped $BaTiO_3$ photocatalyst for photodegradation of tetracycline. *J. Alloys Compd.* **2019**, *774*, 795−802.
(188) Dhanalakshmi, M.; Basavaraj, R. B.; Darshan, G. P.; Sharma, S. C.; Nagabhushana, H. Pivotal role of fluxes in $BaTiO_3$:Eu^{3+} nano probes for visualization of latent fingerprints on multifaceted substrates and anti-counterfeiting applications. *Microchem. J.* **2019**, *145*, 226−234.
(189) Morsi, M. A.; Abdelaziz, M.; Oraby, A. H.; Mokhles, I. Structural, optical, thermal, and dielectric properties of polyethylene oxide/carboxymethyl cellulose blend filled with barium titanate. *J. Phys. Chem. Solids* **2019**, *125*, 103−114.
(190) Lu, X.; Tong, Y.; Cheng, Z. Y. Fabrication and characterization of free-standing, flexible and translucent $BaTiO_3$-P(VDF-CTFE) nanocomposite films. *J. Alloys Compd.* **2019**, *770*, 327−334.
(191) Fu, J.; Hou, Y.; Zheng, M.; Zhu, M. Comparative study of dielectric properties of the PVDF composites filled with spherical and rod-like $BaTiO_3$ derived by molten salt synthesis method. *J. Mater. Sci.* **2018**, *53*, 7233−7248.
(192) Li, J.; Hietala, S.; Tian, X. $BaTiO_3$ supercages: unusual oriented nanoparticle aggregation and continuous ordering transition in morphology. *ACS Nano* **2015**, *9*, 496−502.
(193) Deng, Z.; Meng, G.; Fang, X.; Dong, W.; Shao, J.; Wang, S.; Tong, B. A novel ammonia gas sensors based on p-type delafossite $AgAlO_2$. *J. Alloys Compd.* **2019**, *777*, 52−58.
(194) Mohan, S.; Mao, Y. Hydrothermally Synthesized Copper Gallium Delafossite Nanoflakes for (Photo) Electrocatalytic Water Splitting. *ECS Trans.* **2017**, *77*, 1985−1994.

https://dx.doi.org/10.1021/acs.jpcc.0c10981
J. Phys. Chem. C XXXX, XXX, XXX−XXX

(195) Chen, Y.; Chen, T.; Wu, X.; Yang, G. $CuMnO_2$ nanoflakes as pH-switchable catalysts with multiple enzyme-like activities for cysteine detection. *Sens. Actuators, B* **2019**, *279*, 374−384.
(196) Pokhrel, M.; Gupta, S. K.; Wahid, K.; Mao, Y. Pyrochlore Rare Earth Hafnate $RE_2Hf_2O_7$ (RE = La and Pr) Nanoparticles Stabilized by Molten Salt Synthesis at Low Temperature. *Inorg. Chem.* **2019**, *58*, 1241.
(197) El-Bassuony, A. A. H.; Abdelsalam, H. K. Attractive Improvement in Structural, Magnetic, Optical, and Antimicrobial Activity of Silver Delafossite by Fe/Cr Doping. *J. Supercond. Novel Magn.* **2018**, *31*, 3691−3703.
(198) Cossuet, T.; Resende, J.; Rapenne, L.; Chaix-Pluchery, O.; Jiménez, C.; Renou, G.; Pearson, A. J.; Hoye, R. L. Z.; Blanc-Pelissier, D.; Nguyen, N. D.; Appert, E.; Muñoz-Rojas, D.; Consonni, V.; Deschanvres, J.-L. ZnO/$CuCrO_2$ Core−Shell Nanowire Heterostructures for Self-Powered UV Photodetectors with Fast Response. *Adv. Funct. Mater.* **2018**, *28*, 1803142.
(199) Tong, B.; Deng, Z.; Xu, B.; Meng, G.; Shao, J.; Liu, H.; Dai, T.; Shan, X.; Dong, W.; Wang, S.; Zhou, S.; Tao, R.; Fang, X. Oxygen Vacancy Defects Boosted High Performance p-Type Delafossite $CuCrO_2$ Gas Sensors. *ACS Appl. Mater. Interfaces* **2018**, *10*, 34727−34734.
(200) Nair, B. G.; Joseph, J. A.; Kellner, Z. T.; Sharma, V.; Remillard, S. K.; DeYoung, P. A.; Okram, G. S.; Ganesan, V.; Philip, R. R. Tin-incorporated nanostructured copper indium oxide delafossite thin films: Structural, electrical and optical analysis. *J. Alloys Compd.* **2018**, *746*, 435−444.
(201) Ghosh, C. K.; Popuri, S. R.; Mahesh, T. U.; Chattopadhyay, K. K. Preparation of nanocrystalline $CuAlO_2$ through sol−gel route. *J. Sol-Gel Sci. Technol.* **2009**, *52*, 75−81.
(202) Yamazaki, T.; Morimoto, S.; Hyodo, K.; Ishikawa, T.; Ichiyanagi, Y. Effect of cobalt-doping on the magnetic properties and crystal structure of delafossite $AgFeO_2$ nanoparticles. *J. Alloys Compd.* **2018**, *745*, 631−636.
(203) Huang, G.; Du, X.; Zhang, F.; Yin, D.; Wang, L. A facile molten-salt route for large-scale synthesis of $NiFe_2O_4$ nanoplates with enhanced lithium storage capability. *Chem. - Eur. J.* **2015**, *21*, 14140−14145.
(204) Mouhib, Y.; Belaiche, M.; Briche, S. Elaboration, Characterization, and Magnetic Properties of $Ni_{0.5}Zn_{0.5}Fe_2O_4$ Nanoparticles of High Purity Using Molten Salts Technique. *Phys. Status Solidi A* **2018**, *215*, 1800469.
(205) Preethi, G.; Ninan, A. S.; Kumar, K.; Balan, R.; Nagaswarupa, H. Molten salt synthesis of nanocrystalline $ZnFe_2O_4$ and its photocatalytic dye degradation studies. *Materials Today: Proceedings* **2017**, *4*, 11816−11819.
(206) Zhao, Y.; Cao, B.; Lin, Z.; Su, X. Synthesis of $CoFe_2O_4$/C nano-catalyst with excellent performance by molten salt method and its application in 4-nitrophenol reduction. *Environ. Pollut.* **2019**, *254*, 112961.
(207) Alaparthi, S. B.; Tian, Y.; Mao, Y. Synthesis and photoluminescence properties of $La_2Zr_2O_7$:Eu^{3+}@YBO_3 core@shell nanoparticles. *Nanotechnology* **2014**, *25*, 025703.
(208) Pokhrel, M.; Alcoutlabi, M.; Mao, Y. Optical and X-ray induced luminescence from Eu^{3+} doped $La_2Zr_2O_7$ nanoparticles. *J. Alloys Compd.* **2017**, *693*, 719−729.
(209) Pokhrel, M.; Wahid, K.; Mao, Y. Systematic studies on $RE_2Hf_2O_7$:5%Eu^{3+} (RE = Y, La, Pr, Gd, Er, and Lu) nanoparticles: effects of the A-site RE^{3+} cation and calcination on structure and photoluminescence. *J. Phys. Chem. C* **2016**, *120*, 14828−14839.
(210) Trummel, V.; Gupta, S. K.; Pokhrel, M.; Wall, D.; Mao, Y. Investigating the impact of gamma radiation on structural and optical properties of Eu^{3+} doped rare-earth hafnate pyrochlore nanocrystals. *J. Lumin.* **2019**, *207*, 1−13.
(211) Wahid, K.; Pokhrel, M.; Mao, Y. Structural, photoluminescence and radioluminescence properties of Eu^{3+} doped $La_2Hf_2O_7$ nanoparticles. *J. Solid State Chem.* **2017**, *245*, 89−97.
(212) Wang, Z.; Zhou, G.; Jiang, D.; Wang, S. Recent development of $A_2B_2O_7$ system transparent ceramics. *J. Adv. Ceram.* **2018**, *7*, 289−306.
(213) Mao, Y.; Guo, X.; Huang, J. Y.; Wang, K. L.; Chang, J. P. Luminescent Nanocrystals with $A_2B_2O_7$ Composition Synthesized by a Kinetically Modified Molten Salt Method. *J. Phys. Chem. C* **2009**, *113*, 1204−1208.
(214) Pokhrel, M.; Brik, M. G.; Mao, Y. Particle Size and Crystal Phase Dependent Photoluminescence of $La_2Zr_2O_7$:Eu^{3+} Nanoparticles. *J. Am. Ceram. Soc.* **2015**, *98*, 3192−3201.
(215) Zuniga, J. P.; Gupta, S. K.; Abdou, M.; Mao, Y. Effect of Molten Salt Synthesis Processing Duration on the Photo- and Radioluminescence of UV-, Visible-, and X-ray-Excitable $La_2Hf_2O_7$:Eu^{3+} Nanoparticles. *ACS Omega* **2018**, *3*, 7757−7770.
(216) Gupta, S. K.; Zuniga, J. P.; Abdou, M.; Mao, Y. Thermal annealing effects on $La_2Hf_2O_7$:Eu^{3+} nanoparticles: A curious case study of structural evolution and site-specific photo- and radioluminescence. *Inorg. Chem. Front.* **2018**, *5*, 2508−2521.
(217) Gupta, S. K.; Zuniga, J. P.; Ghosh, P. S.; Abdou, M.; Mao, Y. Correlating Structure and Luminescence Properties of Undoped and $La_2Hf_2O_7$:Eu^{3+} NPs Prepared with Different Coprecipitating pH Values through experimental and theoretical studies. *Inorg. Chem.* **2018**, *57*, 11815−11830.
(218) Pokhrel, M.; Gupta, S. K.; Wahid, K.; Mao, Y. Pyrochlore Rare-Earth Hafnate $RE_2Hf_2O_7$ (RE = La and Pr) Nanoparticles Stabilized by Molten-Salt Synthesis at Low Temperature. *Inorg. Chem.* **2019**, *58*, 1241−1251.
(219) Thi N'Goc, H. L.; Mouafo, L. D. N.; Etrillard, C.; Torres-Pardo, A.; Dayen, J. F.; Rano, S.; Rousse, G.; Laberty-Robert, C.; Calbet, J. G.; Drillon, M.; et al. Surface-Driven Magnetotransport in Perovskite Nanocrystals. *Adv. Mater.* **2017**, *29*, 1604745.
(220) Portehault, D.; Delacroix, S.; Gouget, G.; Grosjean, R.; Chan-Chang, T.-H.-C. Beyond the Compositional Threshold of Nanoparticle-Based Materials. *Acc. Chem. Res.* **2018**, *51*, 930−939.
(221) González-Jiménez, I. N.; Torres-Pardo, A.; Rano, S.; Laberty-Robert, C.; Hernández-Garrido, J. C.; López-Haro, M.; Calvino, J. J.; Varela, Á.; Sanchez, C.; Parras, M.; et al. Multicationic $Sr_4Mn_3O_{10}$ mesostructures: molten salt synthesis, analytical electron microscopy study and reactivity. *Mater. Horiz.* **2018**, *5*, 480−485.
(222) Weller, J. M.; Chan, C. K. Reduction in Formation Temperature of Ta-Doped Lithium Lanthanum Zirconate by Application of Lux-Flood Basic Molten Salt Synthesis. *ACS Applied Energy Materials* **2020**, *3*, 6466−6475.
(223) Huang, X. Preparation and luminescence characteristics of monazite Eu^{3+}:$LaPO_4$ nanocrystals in NH_4NO_3 molten salt. *Opt. Mater.* **2015**, *50*, 81−86.
(224) Wang, B.; Yao, S.; Li, W. Molten-Salt-Assisted Synthesis of $Na_3Bi(PO_4)_2$:Eu^{3+} Nanoparticles with Strong Red Emission. *Phys. Status Solidi A* **2019**, *216*, 1800981.
(225) Golyeva, E.; Tolstikova, D.; Kolesnikov, I.; Mikhailov, M. Effect of synthesis conditions and surrounding medium on luminescence properties of YVO_4:Eu^{3+} nanopowders. *J. Rare Earths* **2015**, *33*, 129−134.
(226) Alshehri, S. M.; Ahmed, J.; Ahamad, T.; Alhokbany, N.; Arunachalam, P.; Al-Mayouf, A. M.; Ahmad, T. Synthesis, characterization, multifunctional electrochemical (OGR/ORR/SCs) and photodegradable activities of $ZnWO_4$ nanobricks. *J. Sol-Gel Sci. Technol.* **2018**, *87*, 137−146.
(227) AlShehri, S. M.; Ahmed, J.; Alzahrani, A. M.; Ahamad, T. Synthesis, characterization, and enhanced photocatalytic properties of $NiWO_4$ nanobricks. *New J. Chem.* **2017**, *41*, 8178−8186.
(228) Amouzegar, Z.; Naghizadeh, R.; Rezaie, H.; Ghahari, M. An investigation on $ZnWO_4$ nano-powder synthesis using $LiNO_3$−KNO_3 medium at low temperature. *Mater. Res. Innovations* **2015**, *19*, 332−337.
(229) Amouzegar, Z.; Naghizadeh, R.; Rezaie, H.; Ghahari, M.; Aminzare, M. Microwave engineering of $ZnWO_4$ nanostructures: towards morphologically favorable structures for photocatalytic activity. *Ceram. Int.* **2015**, *41*, 8352−8359.

https://dx.doi.org/10.1021/acs.jpcc.0c10981
J. Phys. Chem. C XXXX, XXX, XXX−XXX

(230) Mohammadi, A.; Amouzegar, Z.; Aminzare, M.; Jafari, M.; Nasr-Esfahani, M. Synthesis and characterisation of $NiWO_4$ nanopowders via simple molten salt route. *Mater. Res. Innovations* **2017**, *21*, 407−412.
(231) AlShehri, S. M.; Ahmed, J.; Ahamad, T.; Arunachalam, P.; Ahmad, T.; Khan, A. Bifunctional electro-catalytic performances of $CoWO_4$ nanocubes for water redox reactions (OER/ORR). *RSC Adv.* **2017**, *7*, 45615−45623.
(232) Yang, G.; Liang, Y.; Li, K.; Yang, J.; Zhu, Y.; Liu, S.; Xu, R. Comparative study on the synthesis and photocatalytic performance of Bi_2WO_6 nanosheets prepared via molten salt and hydrothermal method. *J. Mater. Sci.: Mater. Electron.* **2018**, *29*, 14311−14321.
(233) Yang, G.; Liang, Y.; Li, K.; Yang, J.; Wang, K.; Xu, R.; Xie, X. Engineering the dimension and crystal structure of bismuth molybdate photocatalysts via a molten salt-assisted assembly approach. *J. Alloys Compd.* **2020**, *844*, 156231.
(234) Li, H.; Wen, P.; Li, Q.; Dun, C.; Xing, J.; Lu, C.; Adhikari, S.; Jiang, L.; Carroll, D. L.; Geyer, S. M. Earth-abundant iron diboride (FeB_2) nanoparticles as highly active bifunctional electrocatalysts for overall water splitting, Advanced Energy. *Materials* **2017**, *7*, 1700513.
(235) Ma, J.-l.; Li, N.; Zhang, Q.; Zhang, X.-b.; Wang, J.; Li, K.; Hao, X.-f.; Yan, J.-m. Synthesis of porous and metallic CoB nanosheets towards a highly efficient electrocatalyst for rechargeable Na−O_2 batteries. *Energy Environ. Sci.* **2018**, *11*, 2833−2838.
(236) Akopov, G.; Roh, I.; Sobell, Z. C.; Yeung, M. T.; Pangilinan, L.; Turner, C. L.; Kaner, R. B. Effects of variable boron concentration on the properties of superhard tungsten tetraboride. *J. Am. Chem. Soc.* **2017**, *139*, 17120−17127.
(237) Akopov, G.; Yeung, M. T.; Kaner, R. B. Rediscovering the crystal chemistry of borides. *Adv. Mater.* **2017**, *29*, 1604506.
(238) Carenco, S.; Portehault, D.; Boissiere, C.; Mezailles, N.; Sanchez, C. Nanoscaled metal borides and phosphides: recent developments and perspectives. *Chem. Rev.* **2013**, *113*, 7981−8065.
(239) Fokwa, B. P.; Misse, P. R.; Gilleßen, M.; Dronskowski, R. Sn-flux syntheses, characterizations and bonding analyses of OsB and TiB_2. *J. Alloys Compd.* **2010**, *489*, 339−342.
(240) Park, H.; Encinas, A.; Scheifers, J. P.; Zhang, Y.; Fokwa, B. P. Boron-dependency of molybdenum boride electrocatalysts for the hydrogen evolution reaction. *Angew. Chem.* **2017**, *129*, 5667−5670.
(241) Ma, J.-l.; Li, N.; Zhang, Q.; Zhang, X.-b.; Wang, J.; Li, K.; Hao, X.-f.; Yan, J.-m. Synthesis of porous and metallic CoB nanosheets towards a highly efficient electrocatalyst for rechargeable Na−O_2 batteries. *Energy Environ. Sci.* **2018**, *11*, 2833−2838.
(242) Khoshsima, S.; Altıntaş, Z.; Schmidt, M.; Bobnar, M.; Somer, M.; Balcı, Ö. Crystalline Co−Fe−B nanoparticles: Synthesis, microstructure and magnetic properties. *J. Alloys Compd.* **2019**, *805*, 471−482.
(243) Choi, S.; Lapitan, L. D., Jr; Cheng, Y.; Watanabe, T. Synthesis of cobalt boride nanoparticles using RF thermal plasma. *Adv. Powder Technol.* **2014**, *25*, 365−371.
(244) Portehault, D.; Devi, S.; Beaunier, P.; Gervais, C.; Giordano, C.; Sanchez, C.; Antonietti, M. A general solution route toward metal boride nanocrystals. *Angew. Chem.* **2011**, *123*, 3320−3323.
(245) Jothi, P. R.; Yubuta, K.; Fokwa, B. P. A simple, general synthetic route toward nanoscale transition metal borides. *Adv. Mater.* **2018**, *30*, 1704181.
(246) Grosjean, R.; Le Godec, Y.; Delacroix, S.; Gouget, G.; Beaunier, P.; Ersen, O.; Ihiawakrim, D.; Kurakevych, O. O.; Chanéac, C.; Portehault, D. A high pressure pathway toward boron-based nanostructured solids. *Dalton Transactions* **2018**, *47*, 7634−7639.
(247) Anasori, B.; Lukatskaya, M. R.; Gogotsi, Y. 2D metal carbides and nitrides (MXenes) for energy storage, Nature Reviews. *Nat. Rev. Mater.* **2017**, *2*, 1−17.
(248) Li, M.; Lu, J.; Luo, K.; Li, Y.; Chang, K.; Chen, K.; Zhou, J.; Rosen, J.; Hultman, L.; Eklund, P.; et al. Element replacement approach by reaction with Lewis acidic molten salts to synthesize nanolaminated MAX phases and MXenes. *J. Am. Chem. Soc.* **2019**, *141*, 4730−4737.
(249) Verger, L.; Xu, C.; Natu, V.; Cheng, H.-M.; Ren, W.; Barsoum, M. W. Overview of the synthesis of MXenes and other ultrathin 2D transition metal carbides and nitrides. *Curr. Opin. Solid State Mater. Sci.* **2019**, *23*, 149−163.
(250) Rasaki, S. A.; Zhang, B.; Anbalgam, K.; Thomas, T.; Yang, M. Synthesis and application of nano-structured metal nitrides and carbides: A review. *Prog. Solid State Chem.* **2018**, *50*, 1−15.
(251) Ressnig, D.; Moldovan, S.; Ersen, O.; Beaunier, P.; Portehault, D.; Sanchez, C.; Carenco, S. An expeditious synthesis of early transition metal carbide nanoparticles on graphitic carbons. *Chem. Commun.* **2016**, *52*, 9546−9549.
(252) Luc, W.; Jiao, F. Synthesis of nanoporous metals, oxides, carbides, and sulfides: beyond nanocasting. *Acc. Chem. Res.* **2016**, *49*, 1351−1358.
(253) Leonard, B. M.; Waetzig, G. R.; Clouser, D. A.; Schmuecker, S. M.; Harris, D. P.; Stacy, J. M.; Duffee, K. D.; Wan, C. Salt flux synthesis of single and bimetallic carbide nanowires. *Mater. Res. Express* **2016**, *3*, 074002.
(254) Ning, S.; Wen, T.; Ye, B.; Chu, Y. Low-temperature molten salt synthesis of high-entropy carbide nanopowders. *J. Am. Ceram. Soc.* **2020**, *103*, 2244−2251.
(255) Pang, Z.; Zou, X.; Li, S.; Tang, W.; Xu, Q.; Lu, X. Molten Salt Electrochemical Synthesis of Ternary Carbide Ti_3AlC_2 from Titanium-Rich Slag. *Adv. Eng. Mater.* **2020**, *22*, 1901300.
(256) Liu, A.; Yang, Q.; Ren, X.; Meng, F.; Gao, L.; Gao, M.; Yang, Y.; Ma, T.; Wu, G. Energy-and cost-efficient NaCl-assisted synthesis of MAX-phase Ti_3AlC_2 at lower temperature. *Ceram. Int.* **2020**, *46*, 6934−6939.
(257) Liu, H.; Wang, Y.; Yang, L.; Liu, R.; Zeng, C. Synthesis and characterization of nanosized Ti_3AlC_2 ceramic powder by elemental powders of Ti, Al and C in molten salt. *J. Mater. Sci. Technol.* **2020**, *37*, 77−84.
(258) Yang, L. X.; Wang, Y.; Zhang, H. L.; Liu, H. J.; Zeng, C. L. A simple method for the synthesis of nanosized Ti_3AlC_2 powder in NaCl−KCl molten salt. *Mater. Res. Lett.* **2019**, *7*, 361−367.
(259) Wan, C.; Zhang, R.; Wang, S.; Liu, X. Molten salt electrolytic fabrication of TiC-CDC and its applications for supercapacitor. *J. Mater. Sci. Technol.* **2017**, *33*, 788−792.
(260) Cheng, H.; Ding, L. X.; Chen, G. F.; Zhang, L.; Xue, J.; Wang, H. Molybdenum carbide nanodots enable efficient electrocatalytic nitrogen fixation under ambient conditions. *Adv. Mater.* **2018**, *30*, 1803694.
(261) Chen, Y.; Wang, X.; Yu, C.; Ding, J.; Deng, C.; Zhu, H.; et al. Low temperature synthesis via molten-salt method of r-BN nanoflakes, and their properties. *Sci. Rep.* **2019**, *9*, 1−11.
(262) Kan, X.; Deng, C.; Yu, C.; Ding, J.; Zhu, H. Synthesis, electrochemical and photoluminescence properties of titanium nitride nanoparticles. *J. Mater. Sci.: Mater. Electron.* **2018**, *29*, 10624−10630.
(263) Kan, X.; Ding, J.; Zhu, H.; Deng, C.; Yu, C. Low temperature synthesis of nanoscale titanium nitride via molten-salt-mediated magnesiothermic reduction. *Powder Technol.* **2017**, *315*, 81−86.
(264) Liang, F.; Tian, L.; Zhang, H.; Liang, F.; Liu, S.; Cheng, R.; Zhang, S. Low temperature synthesis of $LiSi_2N_3$ nanobelts via molten salt nitridation and their photoluminescence properties. *RSC Adv.* **2016**, *6*, 68615−68618.
(265) Liu, H.; Deng, C.; Wang, X.; Yu, C.; Ding, J.; Zhu, H. Low-temperature synthesis and properties of VN nanopowder via a combined molten salt nitridation and magnesium thermal reduction. *Ceram. Int.* **2019**, *45*, 16638−16644.
(266) Örnek, M.; Wang, K.; Xiang, S.; Hwang, C.; Xie, K. Y.; Haber, R. A. Molten salt synthesis of highly ordered and nanostructured hexagonal boron nitride. *Diamond Relat. Mater.* **2019**, *93*, 179−186.
(267) Tian, L.; Li, J.; Liang, F.; Chang, S.; Zhang, H.; Zhang, M.; Zhang, S. Facile molten salt synthesis of atomically thin boron

https://dx.doi.org/10.1021/acs.jpcc.0c10981
J. Phys. Chem. C XXXX, XXX, XXX−XXX

nitride nanosheets and their co-catalytic effect on the performance of carbon nitride photocatalyst. *J. Colloid Interface Sci.* **2019**, *536*, 664−672.
(268) Wang, Y.; Li, Y.; Ju, W.; Wang, J.; Yao, H.; Zhang, L.; Wang, J.; Li, Z. Molten salt synthesis of water-dispersible polymeric carbon nitride nanoseaweeds and their application as luminescent probes. *Carbon* **2016**, *102*, 477−486.
(269) Wang, Y.; Wang, J.; Ma, P.; Yao, H.; Zhang, L.; Li, Z. Synthesis of fluorescent polymeric carbon nitride quantum dots in molten salts for security inks. *New J. Chem.* **2017**, *41*, 14918−14923.
(270) Ye, L.; Zhao, L.; Liang, F.; He, X.; Fang, W.; Chen, H.; Zhang, S.; An, S. Facile synthesis of hexagonal boron nitride nanoplates via molten-salt-mediated magnesiothermic reduction. *Ceram. Int.* **2015**, *41*, 14941−14948.
(271) Zhang, H.; Shih, C.-W.; Martin, D.; Caut, A.; Carlin, J.-F.; Butté, R.; Grandjean, N. Broadened Bandwidth Amplified Spontaneous Emission from Blue GaN-Based Short-Cavity Superluminescent Light-Emitting Diodes. *ECS Journal of Solid State Science and Technology* **2020**, *9*, 015019.
(272) Zhang, M.; Yang, L.; Wang, Y.; Li, L.; Chen, S. High yield synthesis of homogeneous boron doping C_3N_4 nanocrystals with enhanced photocatalytic property. *Appl. Surf. Sci.* **2019**, *489*, 631−638.
(273) Banerjee, D.; Maity, S.; Chattopadhyay, K. Chemically synthesized boron carbon oxynitride as a new cold cathode material. *Chem. Phys. Lett.* **2015**, *641*, 106−111.
(274) Zhou, J.; Zhou, C.; Shi, Z.; Xu, Z.; Yan, S.; Zou, Z. Oriented attachment growth of hundred-nanometer-size $LaTaON_2$ single crystals in molten salts for enhanced photoelectrochemical water splitting. *J. Mater. Chem. A* **2018**, *6*, 7706−7713.
(275) Zhou, P.; Gao, H.; Yan, S.; Zou, Z. The Kirkendall effect towards oxynitride nanotubes with improved visible light driven conversion of CO_2 into CH_4. *Dalton Transactions* **2016**, *45*, 3480−3485.
(276) Fedorov, P.; Mayakova, M.; Alexandrov, A.; Voronov, V.; Kuznetsov, S.; Baranchikov, A.; Ivanov, V. The Melt of Sodium Nitrate as a Medium for the Synthesis of Fluorides. *Inorganics* **2018**, *6*, 38.
(277) Fedorov, P.; Mayakova, M.; Voronov, V.; Baranchikov, A.; Ivanov, V. Preparation of "$NaREF_4$" phases from the sodium nitrate melt. *J. Fluorine Chem.* **2019**, *218*, 69−75.
(278) Garton, G.; Wanklyn, B. Growth of complex flouride single crystals by the flux method. *J. Cryst. Growth* **1967**, *1*, 49−51.
(279) Huang, X.; Jiang, L.; Xu, Q.; Li, X.; He, A. Low-temperature molten-salt synthesis and upconversion of novel hexagonal $NaBiF_4$:Er^{3+}/Yb^{3+} micro-/nanocrystals. *RSC Adv.* **2017**, *7*, 41190−41203.
(280) Huang, X.; Xiong, L.; Qiu, X. Low-temperature route to prepare rare earth fluorides in a molten NH_4NO_3 system: a systematic study on the effects of NaF/Ln ratio and the reaction temperature and time. *CrystEngComm* **2019**, *21*, 182−189.
(281) Ding, M.; Chen, D.; Zhong, J.; Ni, Y.; Lu, C.; Xu, Z.; Ji, Z. Molten Salt Synthesis of β-$NaYF_4$:Yb^{3+},Ln^{3+} (Ln = Er, Tm, and Ho) Micro/Nanocrystals with Controllable Morphology and Multicolor Upconversion Luminescence. *Sci. Adv. Mater.* **2017**, *9*, 688−695.
(282) Fedorov, P.; Alexandrov, A. Synthesis of inorganic fluorides in molten salt fluxes and ionic liquid mediums. *J. Fluorine Chem.* **2019**, *227*, 109374.
(283) Schmitt, A. L.; Higgins, J. M.; Szczech, J. R.; Jin, S. Synthesis and applications of metal silicide nanowires. *J. Mater. Chem.* **2010**, *20*, 223−235.
(284) Zhang, C.; Ni, D.; Liu, Y.; Yao, H.; Bu, W.; Shi, J. Magnesium silicide nanoparticles as a deoxygenation agent for cancer starvation therapy. *Nat. Nanotechnol.* **2017**, *12*, 378−386.
(285) Kumar, R.; Bahri, M.; Song, Y.; Gonell, F.; Thomas, C.; Ersen, O.; Sanchez, C.; Laberty-Robert, C.; Portehault, D. Phase selective synthesis of nickel silicide nanocrystals in molten salts for electrocatalysis of the oxygen evolution reaction. *Nanoscale* **2020**, *12*, 15209−15213.
(286) Liu, H.; Ning, S.; Du, B. Fabrication of High-Entropy Disilicide Nanopowders via Molten Salt-Assisted Magnesium Thermal Reduction. Research Square, 2020, DOI: 10.21203/rs.3.rs-36425/v1.
(287) Godfroy, M.; Russel, A.; Mercier, F.; Granier, M.; Jarrosson, T.; Niebel, C.; Serein Spirau, F.; Viennois, R.; Beaudhuin, M. Nanocrystalline chromium disilicide synthesized by a fast Chlorine-Transfer-Reaction. *Mater. Lett.* **2019**, *247*, 7−10.
(288) Nersisyan, H. H.; Lee, T. H.; Ri, V.; Lee, J. H.; Suh, H.; Kim, J.-G.; Son, H. T.; Kim, Y.-H. NaF-assisted combustion synthesis of $MoSi_2$ nanoparticles and their densification behavior. *J. Phys. Chem. Solids* **2017**, *102*, 34−41.
(289) Ming, L.; Xiufeng, W. Electrolytic synthesis of ZrSi/ZrC nanocomposites from $ZrSiO_4$ and carbon black powder in molten salt. *Int. J. Mater. Res.* **2020**, *111*, 581−586.
(290) Dai, L.; Yu, Y.; Zhou, H.; Yan, X.; Zhu, J.; Li, Y.; Wang, L. In-situ synthesis of $MoSi_2$ coating on molybdenum substrate by electro-deoxidation of a SiO_2 layer in molten salt. *Ceram. Int.* **2015**, *41*, 13663−13670.
(291) Wang, Q.; Zhang, L.; Zhai, L. L.; Li, J. D.; Zhang, J. W. In-situ synthesis of silicide coatings on molybdenum substrates by electrodeposition in chloride-fluoride molten salts. *Int. J. Refract. Hard Met.* **2019**, *82*, 340−348.
(292) Bakshi, M.S.; Ahluwalia, G.K. *Nanostructured chalcogenides, Applications of Chalcogenides: S, Se, and Te*; Springer: 2017; pp 105−157.
(293) Benchikhi, M.; El Ouatib, R.; Er-Rakho, L.; Durand, B. Synthesis and characterization of $CuInS_2$ nanocrystals prepared by solvothermal/molten salt method. *Ceram. Int.* **2016**, *42*, 11303−11308.
(294) Benchikhi, M.; El Ouatib, R.; Er-Rakho, L.; Guillemet-Fritsch, S.; Demai, J. J.; Durand, B. Low-temperature molten salt synthesis and characterization of Cu_2ZnSnS_4 ultrafine powders. *Optik* **2017**, *138*, 568−572.
(295) Jin, H.; Hu, Z.; Li, T.; Huang, L.; Wan, J.; Xue, G.; Zhou, J. Mass Production of High-Quality Transition Metal Dichalcogenides Nanosheets via a Molten Salt Method. *Adv. Funct. Mater.* **2019**, *29*, 1900649.
(296) Kim, J. K.; Jeong, S. Y.; Lim, S. H.; Oh, J. H.; Park, S. K.; Cho, J. S.; Kang, Y. C. Recent Advances in Aerosol-Assisted Spray Processes for the Design and Fabrication of Nanostructured Metal Chalcogenides for Sodium-Ion Batteries. *Chem. - Asian J.* **2019**, *14*, 3127−3140.
(297) Luo, M.; Bu, K.; Zhang, X.; Huang, J.; Wang, R.; Huang, F. Intrinsically low thermal conductivity in a p-type semiconductor $SrOCuBiSe_2$ with a [SrO]-intercalated $CuBiSe_2$ structure. *Chem. Commun.* **2020**, *56*, 4356−4359.
(298) Yang, C.; Wang, Z.; Wu, Y.; Lv, Y.; Zhou, B.; Zhang, W.-H. Synthesis, Characterization, and Photodetector Application of Alkali Metal Bismuth Chalcogenide Nanocrystals, ACS Applied Energy. *Materials* **2019**, *2*, 182−186.
(299) Zhou, X.; Zhao, W.; Pan, J.; Fang, Y.; Wang, F.; Huang, F. Urchin-like Mo_2S_3 prepared via a molten salt assisted method for efficient hydrogen evolution. *Chem. Commun.* **2018**, *54*, 12714−12717.
(300) Wang, W.; Shu, H.; Zhou, D.; Wang, J.; Chen, X. Ultrafast nucleation and growth of high-quality monolayer $MoSe_2$ crystals via vapor-liquid-solid mechanism. *Nanotechnology* **2020**, *31*, 335601.
(301) Yu, H.; Sun, X.; Tang, D.; Huang, Y.; Zhang, W.; Miao, S.; Qiao, Z.-A.; Wang, J.; Zhao, Z. Molten salt strategy to synthesize alkali metal-doped Co_9S_8 nanoparticles embedded, N, S co-doped mesoporous carbon as hydrogen evolution electrocatalyst. *Int. J. Hydrogen Energy* **2020**, *45*, 6006−6014.
(302) Tan, M.; Wang, Z.; Peng, J.; Jin, X. Facile synthesis of large and thin TiS_2 sheets via a gas/molten salt interface reaction. *J. Am. Ceram. Soc.* **2015**, *98*, 1423−1428.
(303) Ghisani, F.; Timmo, K.; Altosaar, M.; Raudoja, J.; Mikli, V.; Pilvet, M.; Kauk-Kuusik, M.; Grossberg, M. Synthesis and characterization of tetrahedrite $Cu_{10}Cd_2Sb_4S_{13}$ monograin material

for photovoltaic application. *Mater. Sci. Semicond. Process.* **2020**, *110*, 104973.
(304) Haynes, A. S.; Lee, K.; Kanatzidis, M. G. One-Dimensional Zinc Selenophosphates: $A_2ZnP_2Se_6$ (A = K, Rb, Cs). *Z. Anorg. Allg. Chem.* **2016**, *642*, 1120−1125.
(305) He, J.; Wang, Z.; Zhang, X.; Cheng, Y.; Gong, Y.; Lai, X.; Zheng, C.; Lin, J.; Huang, F. Synthesis, structure, magnetic and photoelectric properties of $Ln_3M_{0.5}M'Se_7$ (Ln = La, Ce, Sm; M = Fe, Mn; M′ = Si, Ge) and $La_3MnGaSe_7$. *RSC Adv.* **2015**, *5*, 52629−52635.
(306) Masi, A.; Alvani, C.; Angrisani Armenio, A.; Augieri, A.; Celentano, G.; De Marzi, G.; Fabbri, F.; Fiamozzi Zignani, C.; La Barbera, A.; Padella, F.; et al. Fe(Se,Te) system crystallized in molten chlorides flux: The obtained materials and their characterization. *J. Cryst. Growth* **2019**, *528*, 125268.
(307) Ryu, J.; Seo, J. H.; Song, G.; Choi, K.; Hong, D.; Wang, C.; Lee, H.; Lee, J. H.; Park, S. Infinitesimal sulfur fusion yields quasi-metallic bulk silicon for stable and fast energy storage. *Nat. Commun.* **2019**, *10*, 1−9.
(308) Zhong, C.; Weng, W.; Liang, X.; Gu, D.; Xiao, W. One-step molten-salt synthesis of anatase/rutile bi-phase TiO_2@MoS_2 hierarchical photocatalysts for enhanced solar-driven hydrogen generation. *Appl. Surf. Sci.* **2020**, *507*, 145072.
(309) Yang, Z.; Hu, C.; Mutailipu, M.; Sun, Y.; Wu, K.; Zhang, M.; Pan, S. Oxyhalides: prospecting ore for optical functional materials with large laser damage thresholds. *J. Mater. Chem. C* **2018**, *6*, 2435−2442.
(310) Powell, J. M. *Metal oxyhalides and halides for use as electrode materials in Li-ion batteries*. Ph.D. Dissertation, University of Tennessee; 2017).
(311) Li, L.; Han, Q.; Tang, L.; Zhang, Y.; Li, P.; Zhou, Y.; Zou, Z. Flux synthesis of regular Bi_4TaO_8Cl square nanoplates exhibiting dominant exposure surfaces of {001} crystal facets for photocatalytic reduction of CO_2 to methane. *Nanoscale* **2018**, *10*, 1905−1911.
(312) Ogawa, K.; Nakada, A.; Suzuki, H.; Tomita, O.; Higashi, M.; Saeki, A.; Kageyama, H.; Abe, R. Flux Synthesis of Layered Oxyhalide Bi_4NbO_8Cl Photocatalyst for Efficient Z-Scheme Water Splitting Under Visible Light. *ACS Appl. Mater. Interfaces* **2019**, *11*, 5642−5650.
(313) Wang, J.; Li, J.; Wang, K.; Gong, J.; Li, Y.; Zhang, G. Controlled synthesis of Bi_2NbO_5F plates with exposed {010} facet by molten salt method and their photocatalytic mechanism insights. *J. Alloys Compd.* **2019**, *776*, 586−593.
(314) Majumdar, A.; Pal, A. Optimized synthesis of Bi_4NbO_8Cl perovskite nanosheets for enhanced visible light assisted photocatalytic degradation of tetracycline antibiotics. *J. Environ. Chem. Eng.* **2020**, *8*, 103645.
(315) Besara, T.; Ramirez, D. C.; Sun, J.; Falb, N. W.; Lan, W.; Neu, J. N.; Whalen, J. B.; Singh, D. J.; Siegrist, T. Synthesis and Crystal Structure of the Layered Lanthanide Oxychlorides $Ba_3Ln_2O_5Cl_2$. *Inorg. Chem.* **2018**, *57*, 1727−1734.
(316) Zhang, H.; Dasbiswas, K.; Ludwig, N. B.; Han, G.; Lee, B.; Vaikuntanathan, S.; Talapin, D. V. Stable colloids in molten inorganic salts. *Nature* **2017**, *542*, 328−331.
(317) Srivastava, V.; Kamysbayev, V.; Hong, L.; Dunietz, E.; Klie, R. F.; Talapin, D. V. Colloidal Chemistry in Molten Salts: Synthesis of Luminescent $In_{1-x}Ga_xP$ and $In_{1-x}Ga_xAs$ Quantum Dots. *J. Am. Chem. Soc.* **2018**, *140*, 12144−12151.
(318) Hu, Z.; Xiao, X.; Jin, H.; Li, T.; Chen, M.; Liang, Z.; Guo, Z.; Li, J.; Wan, J.; Huang, L.; et al. Rapid mass production of two-dimensional metal oxides and hydroxides via the molten salts method, Nature. *Nat. Commun.* **2017**, *8*, 15630.
(319) Jin, H.; Gu, Q.; Chen, B.; Tang, C.; Zheng, Y.; Zhang, H.; Jaroniec, M.; Qiao, S. Z. Molten Salt-Directed Catalytic Synthesis of 2D Layered Transition-Metal Nitrides for Efficient Hydrogen Evolution. *Chem.* **2020**, *6*, 2382−2394.
(320) Yang, Y.; Qiu, X.; Shi, W.; Hou, H.; Zou, G.; Huang, W.; Wang, Z.; Leng, S.; Ran, Y.; Ji, X. Controllable fabrication of two-dimensional layered transition metal oxides through electrochemical exfoliation of non-van der Waals metals for rechargeable zinc-ion batteries. *Chem. Eng. J.* **2021**, *408*, 127247.
(321) Huang, M.; Yan, Y.; Feng, W.; Weng, S.; Zheng, Z.; Fu, X.; Liu, P. Controllable tuning various ratios of ZnO polar facets by crystal seed-assisted growth and their photocatalytic activity. *Cryst. Growth Des.* **2014**, *14*, 2179−2186.
(322) Jiang, Z.-Y.; Xu, T.; Xie, Z.-X.; Lin, Z.-W.; Zhou, X.; Xu, X.; Huang, R.-B.; Zheng, L.-S. Molten salt route toward the growth of ZnO nanowires in unusual growth directions. *J. Phys. Chem. B* **2005**, *109*, 23269−23273.
(323) Kuang, Q.; Wang, X.; Jiang, Z.; Xie, Z.; Zheng, L. High-energy-surface engineered metal oxide micro-and nanocrystallites and their applications. *Acc. Chem. Res.* **2014**, *47*, 308−318.
(324) Xu, T.; Zhou, X.; Jiang, Z.; Kuang, Q.; Xie, Z.; Zheng, L. Syntheses of nano/submicrostructured metal oxides with all polar surfaces exposed via a molten salt route. *Cryst. Growth Des.* **2009**, *9*, 192−196.
(325) Susman, M. D.; Pham, H. N.; Datye, A. K.; Chinta, S.; Rimer, J. D. Factors governing MgO(111) Faceting in the thermal decomposition of oxide precursors. *Chem. Mater.* **2018**, *30*, 2641−2650.
(326) Wang, X.; Huang, K.; Yuan, L.; Li, S.; Ma, W.; Liu, Z.; Feng, S. Molten salt flux synthesis, crystal facet design, characterization, electronic structure, and catalytic properties of perovskite cobaltite. *ACS Appl. Mater. Interfaces* **2018**, *10*, 28219−28231.
(327) Yan, Y.; Du, J. S.; Gilroy, K. D.; Yang, D.; Xia, Y.; Zhang, H. Intermetallic nanocrystals: Syntheses and catalytic applications. *Adv. Mater.* **2017**, *29*, 1605997.
(328) Kanady, J. S.; Leidinger, P.; Haas, A.; Titlbach, S.; Schunk, S.; Schierle-Arndt, K.; Crumlin, E. J.; Wu, C. H.; Alivisatos, A. P. Synthesis of Pt_3Y and other early−late intermetallic nanoparticles by way of a molten reducing agent. *J. Am. Chem. Soc.* **2017**, *139*, 5672−5675.
(329) Qiu, P.; Bi, J.; Zhang, X.; Yang, S. Organics-and Surfactant-Free Molten Salt Medium Controlled Synthesis of Pt-M (M = Cu and Pd) Bi-and Trimetallic Nanocubes and Nanosheets. *ACS Sustainable Chem. Eng.* **2017**, *5*, 4205−4213.
(330) Gaune-Escard, M., Seddon, K. R. *Molten salts and ionic liquids: never the twain?*; John Wiley & Sons: 2012.
(331) Yau, H. M.; Chan, S. J.; George, S. R.; Hook, J. M.; Croft, A. K.; Harper, J. B. Ionic liquids: just molten salts after all? *Molecules* **2009**, *14*, 2521−2534.
(332) Li, H.; Kobrak, M. N. Instantaneous Normal Mode Analysis of a Series of Model Molten Salts. *ChemPhysChem* **2012**, *13*, 1934−1941.
(333) Pienack, N.; Bensch, W. In-situ monitoring of the formation of crystalline solids. *Angew. Chem., Int. Ed.* **2011**, *50*, 2014−2034.
(334) Parija, A.; Waetzig, G. R.; Andrews, J. L.; Banerjee, S. Traversing Energy Landscapes Away from Equilibrium: Strategies for Accessing and Utilizing Metastable Phase Space, The. *J. Phys. Chem. C* **2018**, *122*, 25709−25728.

https://dx.doi.org/10.1021/acs.jpcc.0c10981
J. Phys. Chem. C XXXX, XXX, XXX−XXX